Water masses in the Atlantic Ocean: water mass ages and ventilation

Mian Liu[1, 2] and Toste Tanhua[2]

[1]School of Environmental Science and Engineering, Xiamen University of Technology, Xiamen, 361021, China

[2]GEOMAR Helmholtz Centre for Ocean Research Kiel, Marine Biogeochemistry, Chemical Oceanography, Wischhofstraße 1-3, 24148 Kiel, Germany

Correspondence to: Mian Liu (2023000069@xmut.edu.cn)

Abstract: The distribution of water masses and their characteristics, including ventilation, provides fundamental insights into large-scale oceanographic processes such as thermohaline circulation and marine biogeochemical cycles. The characteristics of main water masses in the Atlantic Ocean have been comprehensively documented in a companion study (Liu and Tanhua, 2021), this study presents quantitative assessments of water mass age characteristics and ventilation time scales through an analysis using the transient tracers chlorofluorocarbon-12 (CFC-12), sulfur hexafluoride (SF_6), and argon-39 (^{39}Ar). We use two distinct age concepts: mean-age as an integrative metric of water mass chronology, and mode-age as a proxy for advective time scales. Under our fixed transit-time distribution shape ($\Delta/\Gamma = 1$), the two ages are linearly related (mode-age ≈ 0.162·mean-age). Here we mainly report mode-ages; the corresponding mean-ages can be obtained by dividing with 0.162. Empirical results demonstrate systematic age progression with increasing depth and along water mass trajectories. Surface layer central waters exhibit ~~mean ages up to ~100 years and~~ mode ages reaching ~30 years. In the intermediate layer, meridional age gradients characterize the Antarctic Intermediate Water (AAIW) reaching maximum ~~mean-age (~300 years) and~~ mode-age (~80 years) at 30 °N, whereas zonal variations manifest in Mediterranean Water (MW) with peak values (~400 years in mean-age, ~100 years in mode-age) observed in equatorial regions. As the dominant deep water component, North Atlantic Deep Water (NADW) exhibits extreme ages in the Antarctic Circumpolar Current (ACC) region at 50°S, achieving ~~mean age ~600 years and~~ mode age ~100 years. Bottom layer water masses display their oldest signatures: Antarctic Bottom Water (AABW) from the Weddell Sea reaches ~~~600 years mean-age and~~ ~100 years mode-age at equatorial latitudes, while its extension, Northeast Atlantic Bottom Water (NEABW), attains exceptional values of ~~~800 years (mean) and~~ ~120 years ~~(~~mode-age~~)~~ at 50°N. The age analysis reveals significant basin-scale asymmetries, with western basins exhibiting younger ages compared to ~~western~~ eastern counterparts. Ventilation efficiency modulates these age distributions, as evidenced by lower mode-ages and reduced apparent oxygen utilization (AOU) in better-ventilated western basins. The calculated oxygen utilization rate (OUR) demonstrates spatial concordance with dissolved oxygen (DO) concentrations, corroborating enhanced oxidative processes in high-oxygen regimes. This integrated age framework provides novel insights into water mass ventilation dynamics and their biogeochemical implications through quantitative characterization of temporal-spatial age distributions across multiple oceanographic provinces.

Key words: Water Mass, Atlantic Ocean, Transient Tracer, Mean- and Mode-age, Ventilation, GLODAPv2 data product

1 Introduction

The Atlantic Ocean is composed by a complex vertical stratification of water masses characterized by differences in properties such as salinity, temperature and oxygen. Liu and Tanhua (2021) have systematically characterized 16 main water masses that have been extensively considered and studied due to their significant impacts on ocean circulation patterns and global climate regulation (e.g., Hall & Bryden, 1982; Bryden et al., 2005; Kuhlbrodt et al., 2007; Clark et al., 2012). Ocean ventilation constitutes a fundamental thermohaline process responsible for the vertical displacement of surface waters into the deep ocean, effectively redistributing surface heat and salinity anomalies through density-driven stratification. This process inherently obeys the principle of mass conservation, simultaneously enabling the upwelling of deep-sea waters to the surface ocean. The resultant vertical exchange plays a critical role in maintaining global heat distribution patterns and sustaining the thermodynamic equilibrium of the ocean system (Talley, 2013; Armour et al., 2016; Talley et al., 2016). Beyond its thermodynamic significance, ocean ventilation emerges as a pivotal mechanism governing marine biogeochemical cycles. By mediating the downward transport of atmospheric oxygen and carbon dioxide to abyssal depths, this process fundamentally regulates dissolved oxygen concentrations and carbon sequestration rates in the deep ocean (Tanhua et al., 2006; Ziska et al., 2013; Skinner et al., 2017). Related studies have further elucidated ventilation's deterministic role in controlling abyssal redox conditions and organic carbon remineralization processes (van Heuven et al., 2011; Ito et al., 2016; Schmidtko et al., 2017).

Early studies of the water mass ventilation are proposed by Sandström already in the early 20th century (Sandström, 1908; 1916). Sverdrup and Bjerknes also reported the impacts of ventilation and currents on the climate through the air-sea interactions (Sverdrup, 1940; Bjerknes, 1964). Hereafter many studies have been focusing on the ventilation. For instance, Dickson et al., (1994) estimated the formation and pathway of the North Atlantic Deep Water (NADW) based on the hydrodynamics, Orsi et al., (1999) investigated the circulation of the Antarctic Bottom Water (AABW) by using Chlorofluorocarbons (CFCs). Recent studies suggest that the intensity of ocean ventilation varies with environmental factors, such as intensity of the westerly winds (e.g. Rahmstorf, 2010; Purkey et al., 2010; Morrison et al., 2015). Several studies investigate the regional scale or specific water masses, for instance, the upwelling of Circumpolar Deep Water (CDW) in the Southern Ocean (Tamsitt et al., 2017), or the ventilation in the South China Sea (Wang et al., 2021). In parallel, advances in ocean modeling have provided new insights into water mass transformation and tracer transport on basin to global scales, offering valuable perspectives on the climatic drivers of ventilation variability (e.g., Li et al., 2023). However, few studies look at the ventilation over ocean basin scales, which is helpful to understand the effect of ocean-climate interactions, and in addition can provide a basis for the biogeochemical studies.

The water mass age is an important parameter to evaluate the ventilation and refers to as the elapsed time on the pathway. The CFCs and Sulfur hexafluoride (SF_6) are recognized as effective transient tracers for water masses and to estimate their ages, i.e. the time since the water left the surface ocean (Fine, 2011). The concentrations of CFC-12 in surface seawater increased continuously following the increase of the atmospheric concentration since their introduction in the early 20th century (Gammon et al., 1982; Warner and Weiss, 1985) up to about the turn of the century. The use of CFCs as a tracer in the oceanography is well established (e.g. Bullister and Weiss, 1983; Doney and Bullister, 1992; Fine, 2010; 2011), and transient tracers is a core variable in the GO-SHIP repeat hydrography program. Similarly, the transient tracer is an Essential Ocean Variable (EOV) in the Global Ocean Observing System (GOOS) framework. SF_6 has been used as a new tracer since mid-1990s complementing the CFCs due to the reduction of CFCs in the atmosphere (Maiss et al., 1996; Bullister et al., 2002). The application of SF_6 is generally appropriate for recently formed water masses in the upper ocean (Tanhua et al., 2008), i.e. for well ventilated, or young, waters. The CFCs are used to trace the relative deeper water masses (before mid-1990s or partial pressure of CFC-12 lower than about 450 parts per trillion, ppt), while the SF_6 is the better choice for recently formed shallow water masses (after mid-1990s or partial pressure of CFC-12 higher than about 450 ppt, Tanhua et al., 2008). The complementary nature of CFCs and SF_6 allows for more accurate tracing of water masses (Law and Watson, 2001; Vollmer and Weiss, 2002; Watanabe et al., 2003; Tanhua et al., 2004, 2005; Bullister et al., 2006). In addition, the application of transient tracers also provides support to the hydrographic and biogeochemical field in calculating the upwelling velocity (Tanhua and Liu, 2015) or estimating the ventilation and anthropogenic carbon cycle (van Heuven et al., 2011; Tanhua et al., 2013; Patara et al., 2021).

As two typical representatives of transient tracers, the CFC-12 and SF_6 are commonly employed for determining water mass ages, verifying hydrological models, and estimating rates of marine biogeochemical processes, such as anthropogenic carbon storage and oxygen consumption. They exhibit advantages in tracing upper and middle water masses with relatively younger ages. However, challenges arise when attempting to obtain data from deep and bottom layers with old waters. The chemically inert isotope argon-39 (^{39}Ar), which has a half-life of 269 years, addresses this gap. ^{39}Ar is particularly advantageous for tracing deep and bottom water masses with ages exceeding 500 years (Broecker & Peng, 2000; Holzer & Primeau, 2010; Lu et al., 2014). Initially, its application was constrained by the requirement for large sampling volumes—typically around 1000 liters—and the limitations of low-level counting (LLC) detection methods (Loosli et al., 1983; Schlosser et al., 1994; Schlitzer et al., 1985). Consequently, ^{39}Ar was not widely utilized in oceanographic tracer studies. With advancements in Atom Trap Trace Analysis (ATTA) technology (Chen et al., 1999; Jiang et al., 2011), ^{39}Ar has gradually gained prominence as an effective tracer for investigating deep and bottom waters (Lu et al., 2014; Ebser et al., 2018), the accuracy and stability have also been significantly improved (Jia et al., 2025). Therefore, the multi-parameter combination of CFCs, SF_6, and ^{39}Ar can transcend the temporal limitations associated with single-tracer dating methodologies while providing more comprehensive insights into biogeochemical processes. In this study, we introduce ^{39}Ar to investigate water mass ages within the Atlantic Ocean, in particular for the older waters.

The apparent oxygen utilization (AOU, $\mu mol\ kg^{-1}$) is an important indicator in characterizing the respiration of organic matter consuming oxygen, and balancing the oxygen supply through ventilation and photosynthesis. The oxygen utilization rate (OUR, $\mu mol\ kg^{-1}\ yr^{-1}$), which can be calculated from AOU and water mass age, is a significant parameter in estimating the biogeochemical processes such as primary productivity or remineralization (e.g. Jenkins, 1982; Bender, 1990). The OUR has been recognized to be a function of pressure for a long time (e.g. Tseitlin, 1992). However, the OUR is the integrated oxygen consumption rate along the pathway of a water mass and represents a regional view of export flux (e.g. Stanley et al., 2012; Koeve and Kähler, 2016), and thus an imperfect measure of local OUR. In this study, the OUR is calculated from water mass ages estimated from the CFC-12 and SF_6. The change of OUR over time in different water masses are presented and the impacts from the currents and topography are discussed.

In the study by Liu and Tanhua, (2021), the characteristics of main water masses in the Atlantic Ocean are defined by six key properties, using the Global Ocean Data Analysis Project version 2 the annual update 2023 (GLODAPv2.2023, Lauvset et al., 2016; Olsen et al., 2016; Lauvset et al., 2024) data product as a source of unbiased data. The static distribution of the water masses is estimated with the Optimal Multi-Parameter analysis (OMP analysis, Karstensen and Tomczak, 1997; 1998). As a continuation of that work, here we estimate the ventilation of water masses in the Atlantic Ocean with the combination of the above mentioned three transient tracers (CFC-12, SF_6 and ^{39}Ar). The water mass ages are estimated and the OURs are calculated. The goal of this study is to further improve the report of water masses in the Atlantic Ocean by adding the age as a measure of ventilation, and to provide a hydrographic assistant for the biogeochemical researches.

In this article, we start in Section 2 with an overview of the data sources and methodologies employed. Section 3 presents the core results, illustrating the spatial distributions of mean and mode ages for the principal Atlantic Ocean water masses, stratified from surface to bottom. In Section 4, the derived water mass ages are applied to estimate Oxygen Utilization Rates (OUR) and to examine associated biogeochemical implications. Section 5 offers a comparative analysis of water mass ages obtained from traditional transient tracers (CFC-12 and SF_6) and the radioisotope ^{39}Ar. Finally, Section 6 provides a comprehensive summary of conclusions, discusses the broader relevance of the findings, and acknowledges the limitations of the present study.

2 Data and methods

2.1 Transit Time Distribution (TTD) and the Inverse Gaussian Model

To quantify the ventilation timescales of water masses, we apply the Transit Time Distribution (TTD) framework. The TTD, denoted as $G(\tau)$, represents the distribution of transit times τ that water parcels take to travel from the surface formation region to an interior observation point (Hall and Plumb, 1994; Waugh et al., 2003). The concentration of a transient tracer in the ocean interior, $c(t)$, can be modeled as the convolution of its time-evolving atmospheric source function, $c_0(t)$, with the TTD:

$$c(t) = \int_0^{\infty} c_0(t-\tau)G(\tau)d\tau$$

A common and practical parameterization of the TTD is the one-parameter Inverse Gaussian (IG) distribution (Waugh et al., 2003, 2004), which represents a solution to the one-dimensional advection-diffusion equation for a steady-state flow. The IG-TTD is defined as:

$$\mathrm{G}(\tau) = \sqrt{\frac{\Gamma^3}{4\pi\Delta^2\tau^3}}\exp\left(\frac{-\Gamma(\tau-\Gamma)^2}{4\Delta^2\tau}\right);$$

Where:

- τ is the transit time (in years);
- Γ is the mean-age (in years), representing the first moment of the TTD: $\Gamma = \int_0^\infty \tau G(\tau) d\tau$, which signifies the average time elapsed since the water was last in contact with the atmosphere;
- Δ is the width (in years) of the TTD, which quantifies the spread of transit times around the mean age due to mixing and dispersion processes.

The mixing ratio, defined as (Δ/Γ, unitless), indicates the relative importance of mixing versus advection in the transport. A low ratio ($\ll 1$) suggests advection-dominated transport with a narrow range of transit times, while a high ratio ($\gg 1$) indicates strong mixing and a wide range of transit times.

While other forms of TTD, for instance, a two-IG distribution to characterize a mix of two water masses with different TTSs was used by Stöven and Tanhua (2014) for the Mediterranean Sea, or non-steady-state circulations may better represent reality in certain regions, the one-parameter IG-TTD remains a widely adopted and practical model. This is particularly true given the typical scarcity of multiple, independent tracer observations needed to constrain more complex distributions across large ocean basins. In this study, we apply the one-parameter IG-TTD framework as a robust approach for basin-scale analysis.

2.2 Definitions of Water Mass Age: Tracer-age, Mean-age, and Mode-age

The fundamental concept of water mass age is the time elapsed since a water parcel was last in equilibrium with the atmosphere at the surface (Thiele and Sarmiento, 1990). From the TTD framework, we derive and utilize three specific age definitions, each with its own physical interpretation and application (see conceptual diagram in Fig. 1).

Tracer-age is the simplest age estimate, obtained by matching the observed tracer partial pressure in a water sample directly to the historical atmospheric record (Fig. 1 a). It assumes the transport along a purely advective pathway (i.e., no mixing), corresponding to a TTD that approaches a delta function as $\Delta/\Gamma \to 0$. This concept systematically underestimates the "true" age in the presence of mixing, as it ignores the distribution of transit times/pathways (Sonnerup et al., 2001).

Mean-age (Γ) is the first moment of the TTD. The mean-age represents the average value of the transport times of all water parcel and represents an integrative timescale (Fig. 1 b), particularly applicable to the study of biogeochemical accumulation processes, such as calculating integrated oxygen consumption rates (e.g., Jenkins, 1987; Sonnerup et al., 2013).

Mode-age (τ_{mode}) is the transit time at which the TTD, G(t), reaches its maximum (Fig. 1 b). For the IG-TTD, it is calculated as $\tau_{mode} = \Gamma \bullet \left(\sqrt{1 + (3\Delta/\Gamma)^2} - 3\Delta/\Gamma\right)$, with the mixing ratio fixed at $\Delta/\Gamma = 1$ in this study, this simplifies to $\tau_{mode} = \Gamma \bullet (\sqrt{10} - 3) \approx 0.162 \bullet \Gamma$. The mode-age represents the most probable transit time of the dominant water fraction in the sample, making it a better proxy for the advective timescale along the core pathway of a water mass.

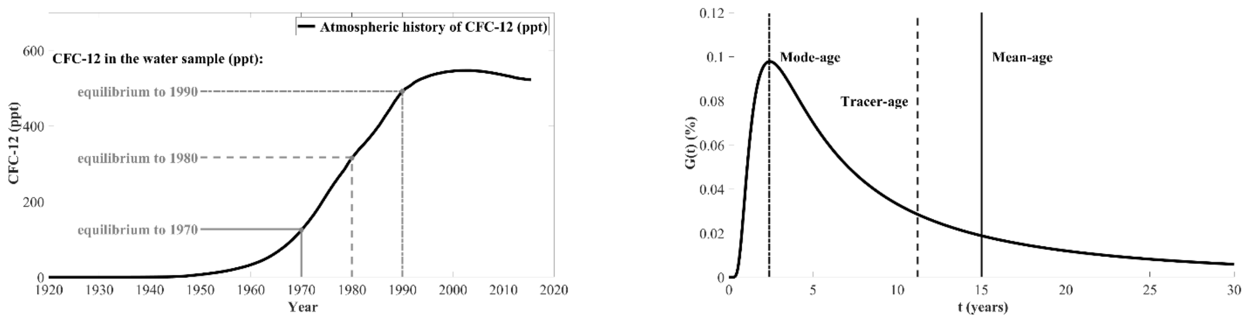

(a) (b)

Figure 1. Schematic diagram illustrating three concepts of water mass ages.
(a) The tracer age: The transient tracer (such as CFC-12) in the water sample in equilibrium with the atmospheric at a certain year-This approach and assumes that the ocean is a purely advective process (without mixing);
(b) The concepts of mean- and mode-ages: Based on the inverse Gaussian transport time distribution model, assuming the mixing ratio ($\Delta/\Gamma = 1$) and observed tracer partial pressure CFC-12 = 300 ppt, as an example. Shown are the positions of the mean-age (Γ), tracer age, and the mode-age (τ_{mode}).

To calculate tracer partial pressures from measured concentrations, the saturation of transient tracers (CFC-12 and SF_6) in surface seawater must be determined. This saturation is a function of potential temperature (θ) and practical salinity (S), following established solubility relationships (Warner and Weiss, 1985; Bullister et al., 2002).

2.3 Determination of the Mixing Ratio and age calculation procedure

A critical step in applying the IG-TTD is specifying the shape parameter, the mixing ratio (Δ/Γ). The atmospheric concentrations of these tracers provide the essential input for age calculations: the CFC-12 increased monotonically until mid-1990s, while the SF_6 is still increasing (Fig. 2a). Ideally, the mixing ratio is determined by fitting the TTD model to observations of two or more transient tracers with different input histories. However, the similar atmospheric growth curves of CFC-12 and SF_6 often preclude a robust, independent determination of Δ/Γ across large ocean basins (Waugh et al., 2004), and the short atmospheric history of SF_6 reduce this method to recently ventilated waters. Furthermore, the limited number of collocated transient tracer observations restricts the application of more complex models. In this context, understanding how the mixing ratio influences age estimates is crucial. For instance, under given tracer partial pressure (e.g., CFC-12 = 300 ppt) and sampling year (e.g., 1990), an increase in the Δ/Γ ratio of the IG-TTD leads to a corresponding increase in the calculated mean-age, while the mode-age decreases. This behavior arises from the shape of the Inverse Gaussian distribution: a higher mixing ratio extends the distribution's tail, elevating the mean-age, while simultaneously shifting its peak earlier, thereby reducing the mode-age (Fig. 2b). Observational evidence from hydrographic sections further supports this theoretical relationship, demonstrating how the resulting age fields vary systematically under different assumed mixing ratios (Fig. 3)

To ensure a consistent and widely comparable analysis across the whole Atlantic Ocean, we adopt the standard mixing ratio $\Delta/\Gamma = 1$. This value represents a balance between advective and diffusive processes and is commonly used in large-scale oceanographic studies (Waugh et al., 2004; Stanley et al., 2012; Stöven and Tanhua, 2014; Thomas et al., 2020). We acknowledge this as a limitation but note it is a necessary and widely accepted approach for basin-scale analyses where tracer data are limited. Because this study adopts a fixed mixing ratio ($\Delta/\Gamma = 1$), the mean-age and mode-age are strictly linearly related ($\tau_{mode} \approx 0.162 \cdot \Gamma$). They therefore do not provide independent statistical information. Nevertheless, we present both age concepts in this manuscript because they carry different physical interpretations: mean-age is an integrative timescale (average over all pathways), whereas mode-age is a proxy for the advective timescale (most probable transit time along the core pathway). Presenting both allows readers to intuitively compare the magnitudes of "average" versus "most probable" travel times. In all subsequent analyses that require a single age metric (e.g., OUR calculation in Section 4), we use the mode-age. The linear relationship is explicitly noted in the captions of figures where both ages are shown.

The mean-age (Γ) for each sample was calculated by finding the value that minimizes the difference between the observed tracer partial pressures and those predicted by convolving the IG-TTD (with $\Delta/\Gamma = 1$) with the atmospheric histories of CFC-12 and SF_6. The atmospheric histories for the Northern Hemisphere were taken from Bullister et al., (2002). Where both CFC-12 and SF_6 data were available, they were used jointly in the inversion. Following Tanhua et al. (2008), in waters where the CFC-12 partial pressure was above ~450 ppt (typically younger, shallower waters), the solution relied more heavily on SF_6, whereas CFC-12 was the primary tracer used at lower partial pressures (typically older, deeper waters). The corresponding mode-age was then calculated from the derived mean-age and the fixed mixing ratio. For the radioactive tracer ^{39}Ar, the convolution integral incorporates an additional exponential decay term, $\boldsymbol{e^{-\lambda t}}$, where $\boldsymbol{\lambda}$ is the decay constant corresponding to its 269-year half-life.

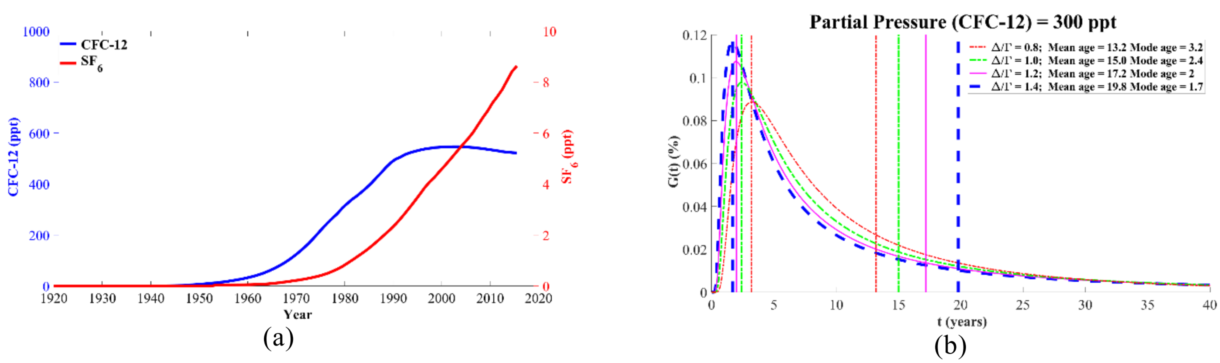

Figure 2. The relationships between mean-age, mode-age and mixing ratio (Δ/Γ).
(a) Historical atmospheric partial pressure data of transient tracers over time (CFC-12 and SF_6) in the Northern Hemisphere (data source: Bullister, 2002);
(b) Relationship between mean-ages and mode-ages under same partial pressure (CFC-12 = 300 ppt) but different mixing ratios (Δ/Γ) assuming the sampling year is 1990.

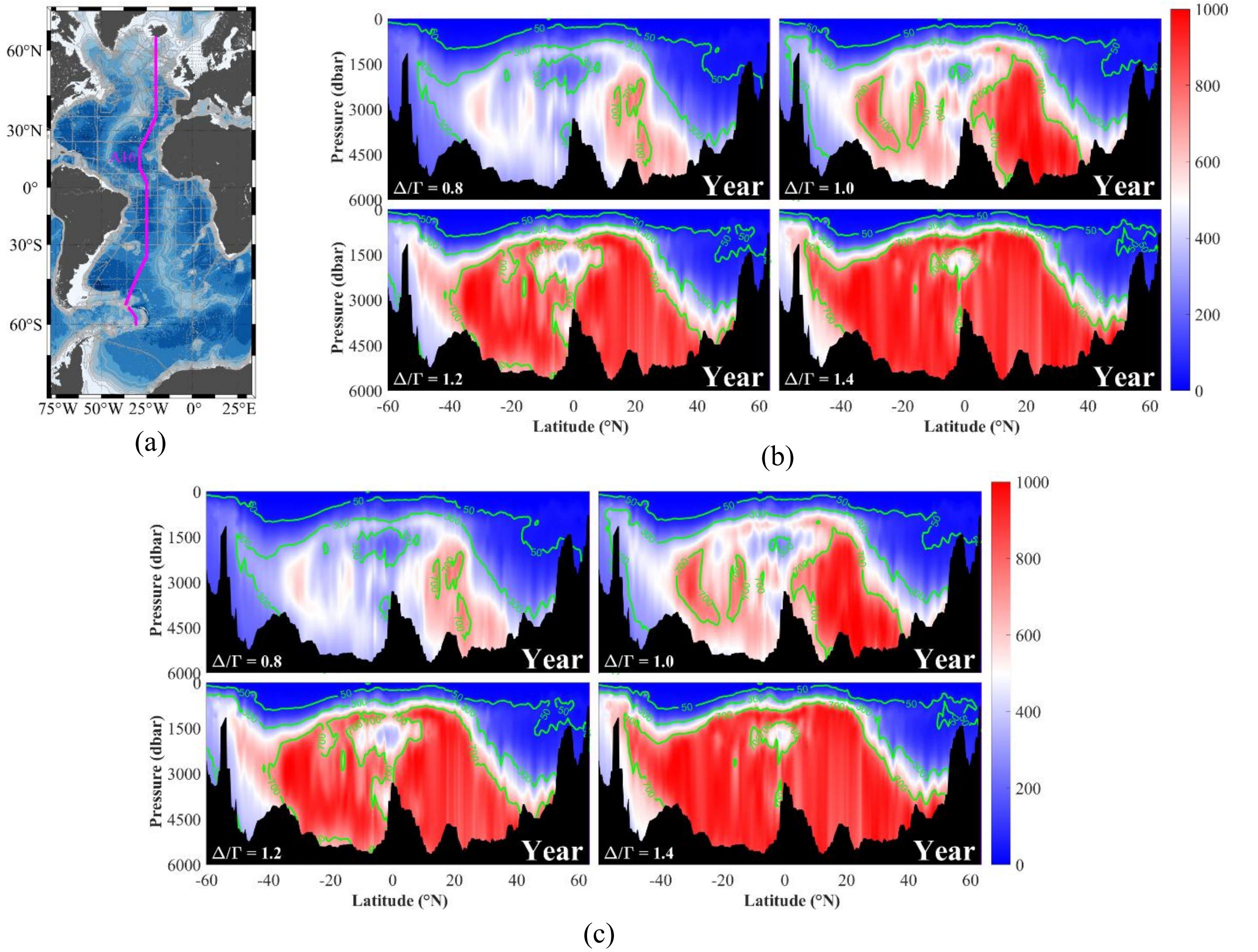

Figure 3. (a) Map of the A16 section under the framework of the WOCE/GO-SHIP project in 2013. (b) Distributions of mean-ages and (c) mode-ages under varying mixing ratios (ΔΓ = 0.8, 1.0, 1.2, and 1.4) derived from GLODAPv2 observational data. Green contour lines correspond to mean-ages of 50, 300, and 700 years and mode-ages of 50, 100, and 150 years, respectively.

3 Results: Ages of water masses in the Atlantic Ocean

As established in Section 2.3, under the fixed mixing ratio ($\Delta/\Gamma = 1$), the mode-age is a constant fraction of the mean-age. Therefore, the spatial patterns of the two age-metrics are identical, differing only in numerical scale. To avoid redundancy while preserving the information, the mode-age sections (corresponding to Fig. 5–13) are provided in the Supplement (Figs. S1–S9). In the following, we present only the mean-age distributions; the mode-age can be readily derived from the mean-age if needed, and is used for OUR calculations in Section 4.

In this study, we follow the division of vertical layers and distributions of water masses presented by Liu and Tanhua (2021), but now focus on the transient tracers and water mass ages. Three hydrographic sections are selected from the WOCE/GO-SHIP sections in this work to represent the mean-ages of the main water masses (Table 1). The A16 sections in 2013 (Expo-code 33RO20130803 and 33RO20131223) show the meridional distribution across the whole Atlantic Ocean, while the A05 section in 2010 (Expo-code 74DI20100106) and A10 section in 2011 (Expo-code 33RO20110926) show the zonal distributions in the North and South Atlantic Ocean respectively (Fig. 4). The partial pressures of CFC-12 and SF_6 along the above sections are shown in Fig. 4 (Only CFC-12 data are displayed along A05 section due to the lack of SF_6 data in this section). Both tracers show similar distributions with high values in the shallow layers, and a general decrease with increasing pressure.

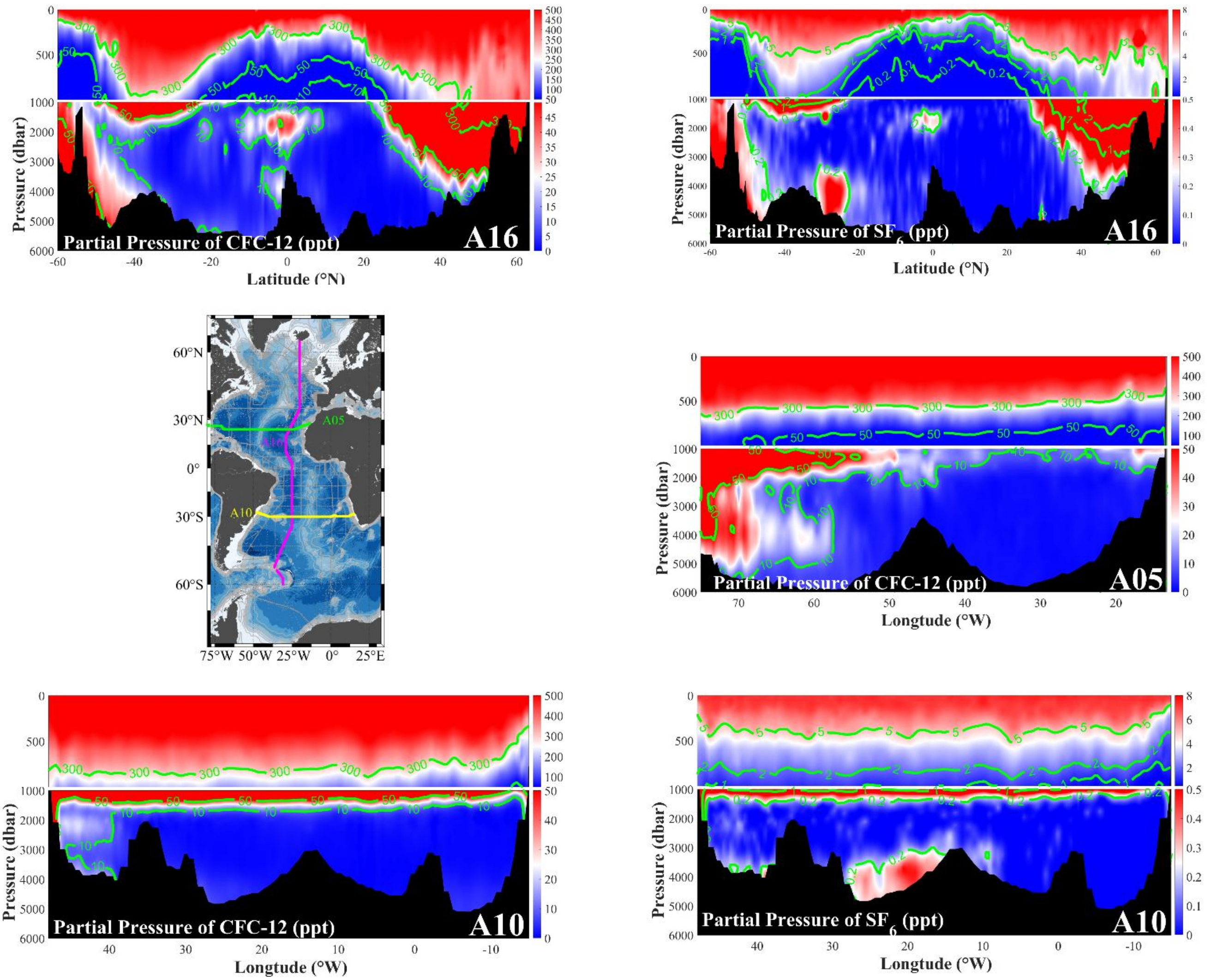

Figure 4. Map of three selected WOCE/GO-SHIP sections to represent the ages of the main water masses in the Atlantic Ocean (middle left) and partial pressures of CFC-12 and SF_6 along the three selected sections. Note the different colorbars between upper and lower parts divided at pressure of 1000 dbar. The green contour lines indicate the partial pressures of CFC-12 at 10, 50 and 300 ppt and SF_6 at 0.2, 1, 2 and 5 ppt, respectively.

Table 1: Summary of hydrographic cruises in the Atlantic Ocean selected for the oceanographic sections in this study

WOCE/GO-SHIP section	Year	Expo-code	Ship	Chief Scientist	PI of transient tracers
A16N	2013	33RO20130803	Ronald H. Brown	John Bullister & Molly Baringer	John Bullister
A16S	2013	33RO20131223	Ronald H. Brown	Rik Wanninkhof	John Bullister
A05	2010	74DI20100106	Discovery	Brian King	Marie-José Messias
A10	2011	33RO20110926	Ronald H. Brown	Molly Baringer	John Bullister

The upper water layers have the lowest mean-ages within ~100 years and mode-ages within ~30 years (Fig. 5), the surface water has, by definition, zero age. The distributions of mean-ages and mode-ages also show spatial differences in the horizontal direction. Relatively low ages are found in the high latitude regions (Fig. 5, a and b). This indicates that the deep water masses are newly formed here, and thus have low ages. In the region between 20 and 40 °N, ~~the mean-age reaches the peak value up to ~1000 years and~~ the mode-age up to ~150 years, suggesting the sluggish water exchange and long residence time of old water masses. In the zonal direction, both mean-ages and mode-ages are significantly lower in the west in the general region below 1500m dbar, suggesting that these regions are better ventilated due to the western boundary current (Fig. 5 c to f).

In the analysis of water mass ages in each layer, maps with mean-ages and mode-ages in each station are firstly presented as a qualitative overview. The mean values of the ages at the core pressure of each water mass are plotted at certain station. In addition, the quantitative calculations are made along the three selected sections to represent the distributions of water mass ages in detail and estimate the impacts from currents and mixing.

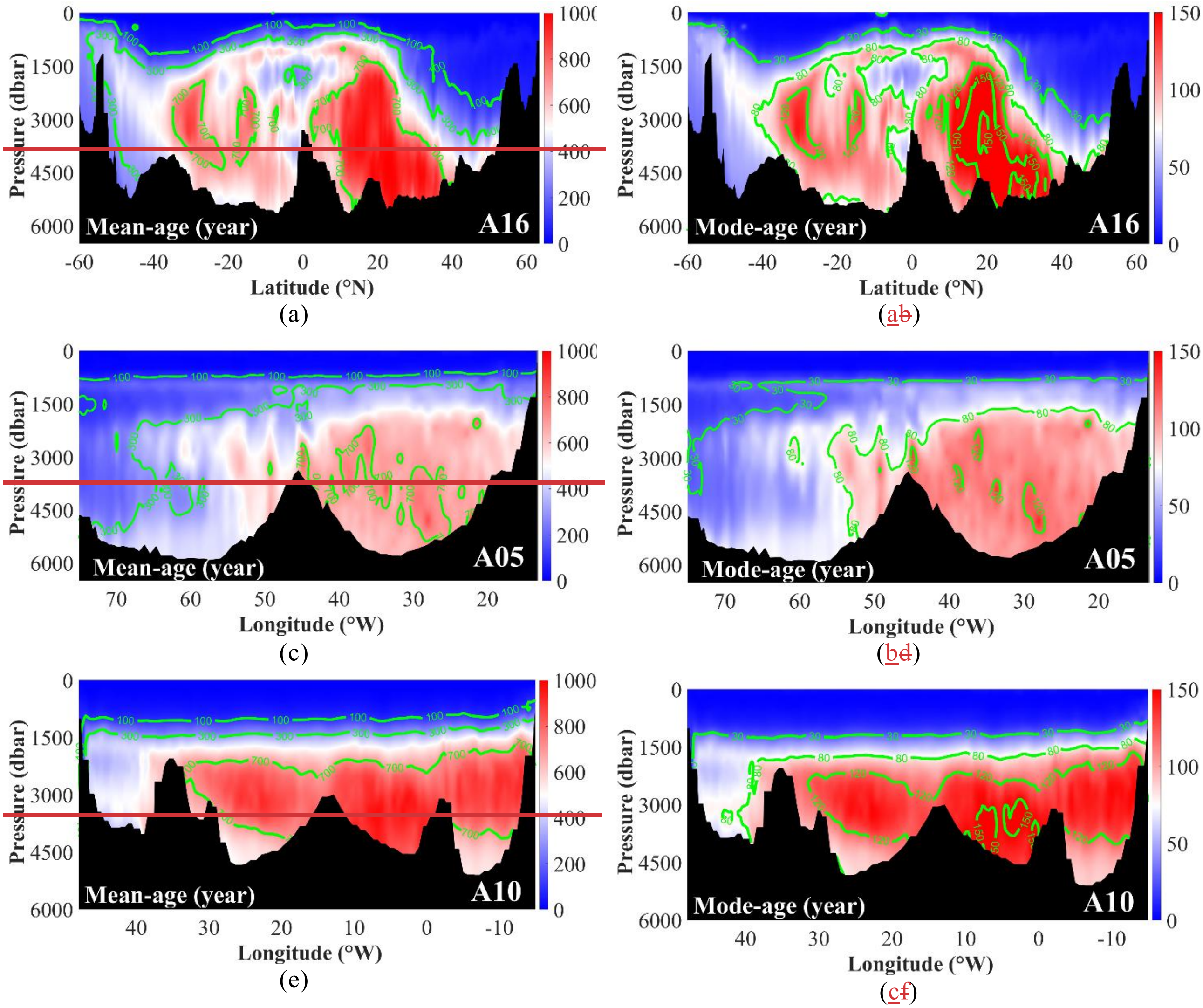

Figure 5. ~~Mean-ages and~~ Mode-ages along the three selected WOCE/GO-SHIP sections

3.1 The upper layer

The spreading of central waters can be traced by the distributions of ages. After leaving their formation areas in the mid-latitude regions, the West North Atlantic Central Water (WNACW) and West South Atlantic Central Water (WSACW) spread generally in zonal direction towards the formation areas of the East North Atlantic Central Water (ENACW) and East South Atlantic Central Water (ESACW) with Azores Current and South Atlantic Current, respectively (Fig. 6, a). The mean -ages show that the "mixed" age of all the compositions in the western central waters is ~50 years (Fig. 6, b and Fig. 7). When focusing on the main body of WNACW and WSACW, the mode-ages show that the advective time-scale is ~15 years for both water masses (i.e. Both WNACW and WSACW take ~15 years from the formation area to the equator, Fig. 6, c and Fig. 7).

At greater depths, the ENACW and ESACW are transported from their formation areas and spread with the main currents towards the equator (Fig. 6, a). In the northern hemisphere, the ENACW spreads southward with the Canaries Current, while the ESACW in the southern hemisphere is transported northward with the Benguela Current and the South Equatorial Current. The difference in mean-age is ~100 years between the formation areas and the equatorial region (Fig. 6, b and Fig. 7). The mode-ages indicate that the main body of ENACW and ESACW takes approximately 30 years to be transported from formation areas to the equator (Fig. 6, c and Fig. 7).

The central waters occupy the upper layer above the neutral density isoline of 27.10 kg m^{-3}. The core pressures of western and eastern central waters are around the neutral density (γ) of 26.5 and 26.9 kg m^{-3} respectively (Liu and Tanhua, 2021). The ages of central waters at their core neutral densities are shown in Fig. 6. The eastern central waters have mean-ages of up to approximately 100 years and mode-ages up to approximately 30 years, while the western central waters are younger with ages of ~50 years and ~15 years respectively (Fig. 6). The relatively low ages in the upper layer indicate that these water masses are newly formed.

In the meridional direction along the A16 section, ~~both mean-ages and~~ mode-ages show low values of around 20 years in the mid-latitude regions that are close to the formation areas of central waters (Fig. 6 and Fig. 7). In contrast, the ages are higher (~~~100 years for mean-age and~~ ~30 years for mode-ages) in the tropical region. In the zonal direction, the ages in the eastern basin are slightly higher than in the western basin for the central waters, but the difference is only within ~10 years for both mean-ages and mode-ages, indicating that the influence from western boundary current is not significant in the upper layer (Fig 7).

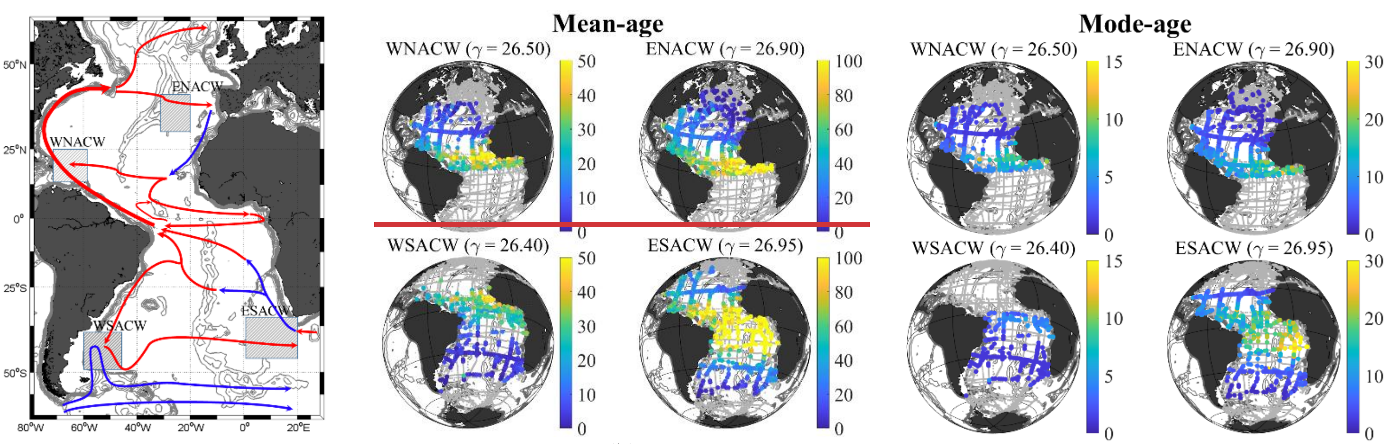

(a) (b) (c)

Figure 6. Ages of central water masses in the Atlantic Ocean.
(a) The main currents in the upper layer with warm (red) and cold (blue) currents and the approximate formation areas (rectangular shadows) of central water masses.
(b) The mean- and (c) mode-ages of central water masses at their core neutral densities (kg m^{-3}). The colored dots show the ages in each station. The grey dots show all the GLODAPv2 stations that have less than 20% contribution of the water mass in question or lack of transient-tracer data.

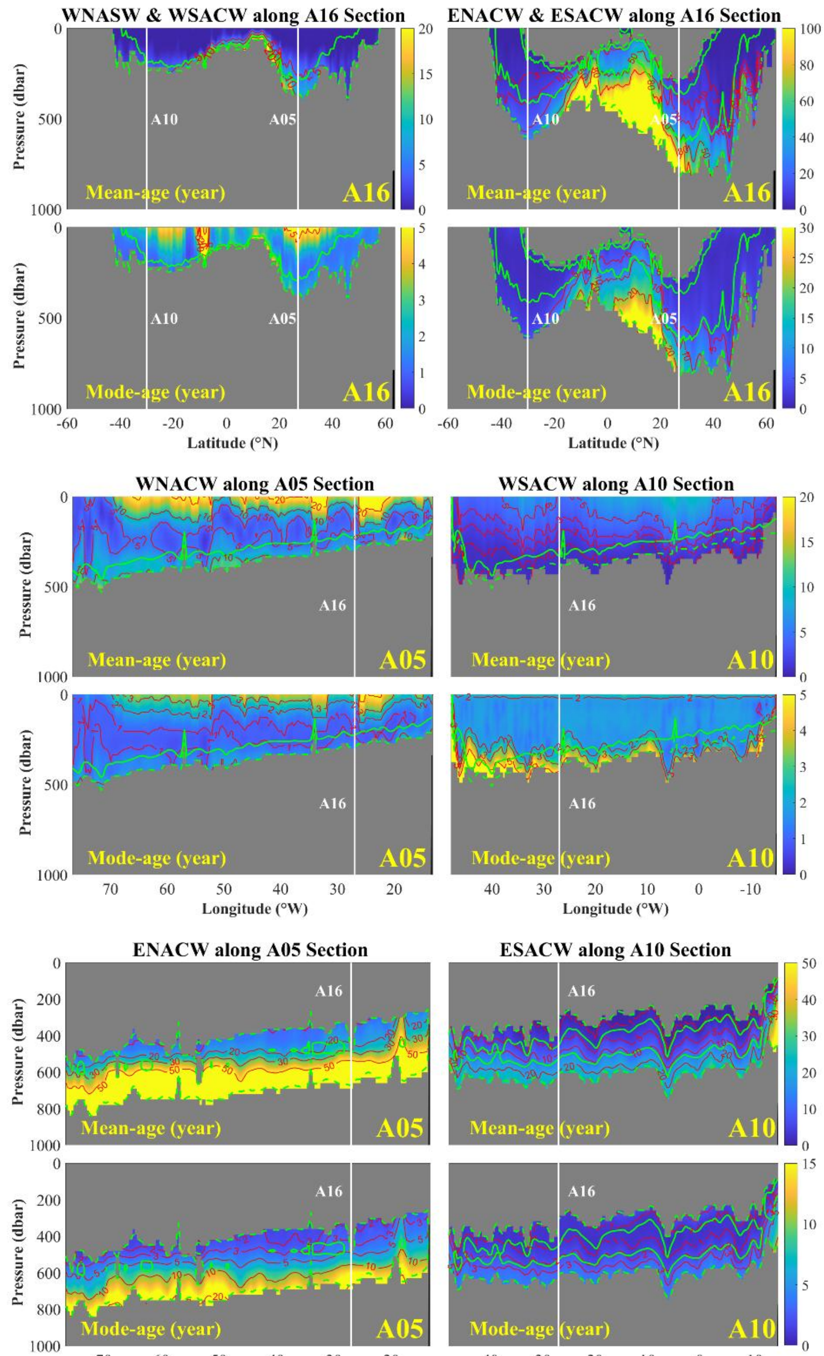

Figure 7. The mean- and mode-ages of central waters along the three sections for the upper 1500 dbar. The solid green isolines show the 50% fractions of water masses and the dashed green lines show the 20 % fractions. The grey color indicate areas with less than 20% contribution from central waters. White vertical lines show cross overs with other sections.

3.2 The Intermediate Layer

Three main water masses belong to the intermediate layer (γ between 27.10 and 27.90 kg m^{-3}), including the Antarctic Intermediate Water (AAIW), the Subarctic Intermediate Water (SAIW) and the Mediterranean Water (MW). The ages of SAIW are not displayed in this study due to the lack of tracer data with a complete section through the distribution region of this water mass.

Antarctic Intermediate Water (AAIW): The AAIW spreads from the formation area between 40 and 50 °S northward to approximately 30 °N along the Western Boundary Current (WBC) (Fig. 8, a). The northward flow of this water mass is part of the Atlantic western boundary current system (Talley, 1996) and the upper limb of AMOC (Kirchner et al., 2009).

Compared to the central waters, AAIW has significantly higher ages. In principle, the AAIW is supposed to get higher ages towards the north, as the transport time increases with the distance from the formation area in the south. In the meridional direction, the ~~mean- and~~ mode-ages increases from 0 to ~~~300 years and~~ ~80 years from formation area to the equator, and further increase up to ~~~400 years and~~ ~100 years respectively to 20 °N (Fig. 8 and 9). However, ~~both~~ mode ages decrease instead and approach even towards 0 in the further north region between 20 °N and 30 °N (Fig 8, b and c), giving the impression of the AAIW being younger in the north Atlantic Ocean. The observed decrease in ages likely results from mixing with younger surrounding water masses, although other factors such as limitations of the steady-state IG-TTD assumption (e.g., Waugh et al., 2004) or regional variations in the mixing ratio (e.g., Thomas et al., 2020) may also contribute. The maximum distance of AAIW to the north can reach 30 °N. However, the mixing is speculated between 20 °N and 30 °N, since the ENACW and upper NADW comes into contact with AAIW from the upper and lower (Liu and Tanhua, 2021) (Fig 7, a, Fig. 9, a and Fig. 11, a). Both ENACW and upper NADW are newly formed in this region, so the "mixed" AAIW obtains younger ages. Age differences are also found in the zonal direction. In better ventilated western basins, the AAIW transports northward with the western boundary current (WBC), so the mean- and mode-ages are lower. By contrast, the ages are significantly higher in the eastern basins with poor ventilation. The `~~mean-ages reach ~400 years and the~~ mode-ages are up to ~100 years in the east between 0 and 20 °S (Fig. 8, b and c). The mean- and mode-ages along the A05 section also show the zonal difference (Fig. 9, b). In the eastern basin (east of the Mid-Atlantic-Ridge, MAR), the mean-age and mode-age appears up to ~400 and ~80 years respectively, in contrast only ~200 years and ~50 years in the west. This distribution confirms that the AAIW is transported by the WBC and takes a longer time to cross the MAR. Generally lower ages are found along the A10 Section in contrast to the A05 Section due to closer distance to the formation area of AAIW (Fig. 9, c). Similar zonal difference exists with ~~mean-ages of ~50 years in the west ~100 years in the east and~~ mode-age of ~10 years in the west and ~ 20 years in the east.

Both mean- and mode-ages of AAIW also vary in the vertical direction. These variations are consistent with the influence of mixing with adjacent water masses along its boundaries. Near the upper boundary, the AAIW is characterized by relatively lower ages, which is consistent with mixing with the generally younger eastern central waters above. Conversely, at the lower boundary with the deep and overflow layer, AAIW encounters the southward upper NADW. Along the A10 section, the upper

NADW exhibits high ~~mean-ages (~600 years) and~~ mode-ages (~80 years) due to the long southward transport. The resulting composite water mass at this interface shows intermediate ages (~~~300 years mean-age,~~ ~60 years mode-age), higher than those in the AAIW core (~100 years mean-age, ~20 years mode-age) (Fig. 9 c).

A contrasting pattern is observed along the A05 section. In the northern Atlantic sampled by A05, the AAIW obtains higher water mass ages, while the locally encountered upper NADW is relatively younger. Consequently, the ages at the interface (~~~200 years mean-age,~~ ~50 years mode-age) are lower than those in the AAIW core at this location (~~~300 years mean-age,~~ ~60 years mode-age) (Fig. 9 b). These observed patterns at the boundaries are interpreted as reflecting the mixing of AAIW with water masses of contrasting ages, and the resulting composite age signals are consistent with the independent age estimates for NADW presented in the following section.

Mediterranean Water (MW): The MW is referred to as the product of the Mediterranean Overflow Water (MOW) that flows across the Strait of Gibraltar and mixes with the ENACW (Liu and Tanhua, 2021). This water mass is formed in the Gulf of Cadiz where the MOW exits the Strait of Gibraltar as a deep current and turns into two branches (Fig 8, a). The northward branch spreads into the West European Basin until 50 °N, while the westward branch spreads across the MAR into the west basin of the North Atlantic Ocean (Price et al., 1993; Carracedo et al., 2016).

The spreading of MW can also be traced by the transient tracers (Fig 9, a), in addition to the water mass variables that goes into the OMP analysis (Liu and Tanhua, 2021). The ages of MW have an increasing trend towards the south (Fig. 8, b and c). The northward flow spreads faster so the ~~mean-age is ~100 years and the~~ mode-age is ~ 20 years at 50 °N. In contrast, the southward flow shows a higher ~~mean-age of ~400 years and~~ mode-age of ~100 years at 25 °N along the A05 Section (Fig 9, b). In the zonal direction, the ages decrease to the west (Fig 9, b), since the fraction of MW is only between 20% and 30% along this section (green dash contour lines in Fig 9, b), and is therefore influenced by the lower ages from the NADW.

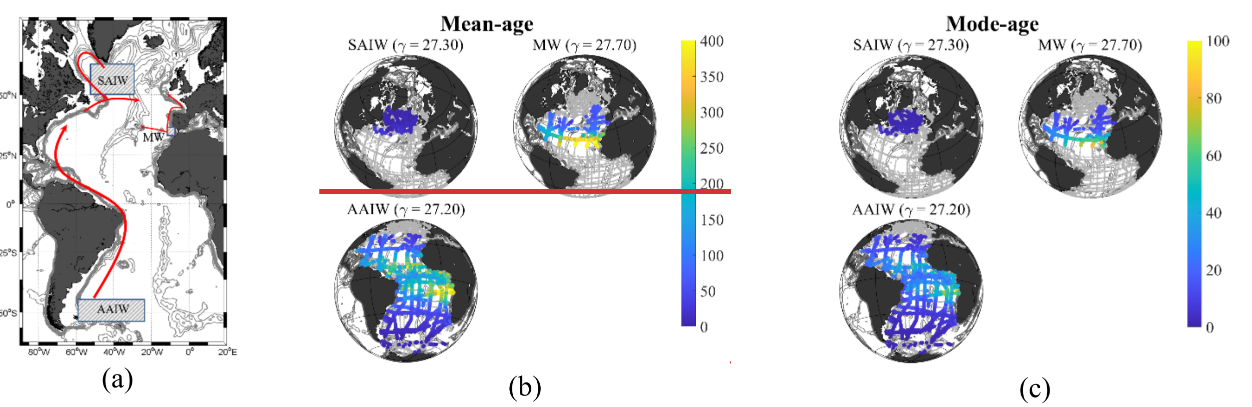

Figure 8. Ages of intermediate water masses in the Atlantic Ocean.
(a) Main currents in the intermediate layer. The currents (arrows) and the formation areas (rectangular shadows) of water masses in the intermediate layer.
(b) The ~~mean- and (c)~~ mode-ages of intermediate water masses at their core neutral densities (kg m^{-3}). The colored dots show the ages in each station. The grey dots show all the GLODAPv2 stations that have less than 20% contribution of the water mass in question or lack of transient-tracer data.

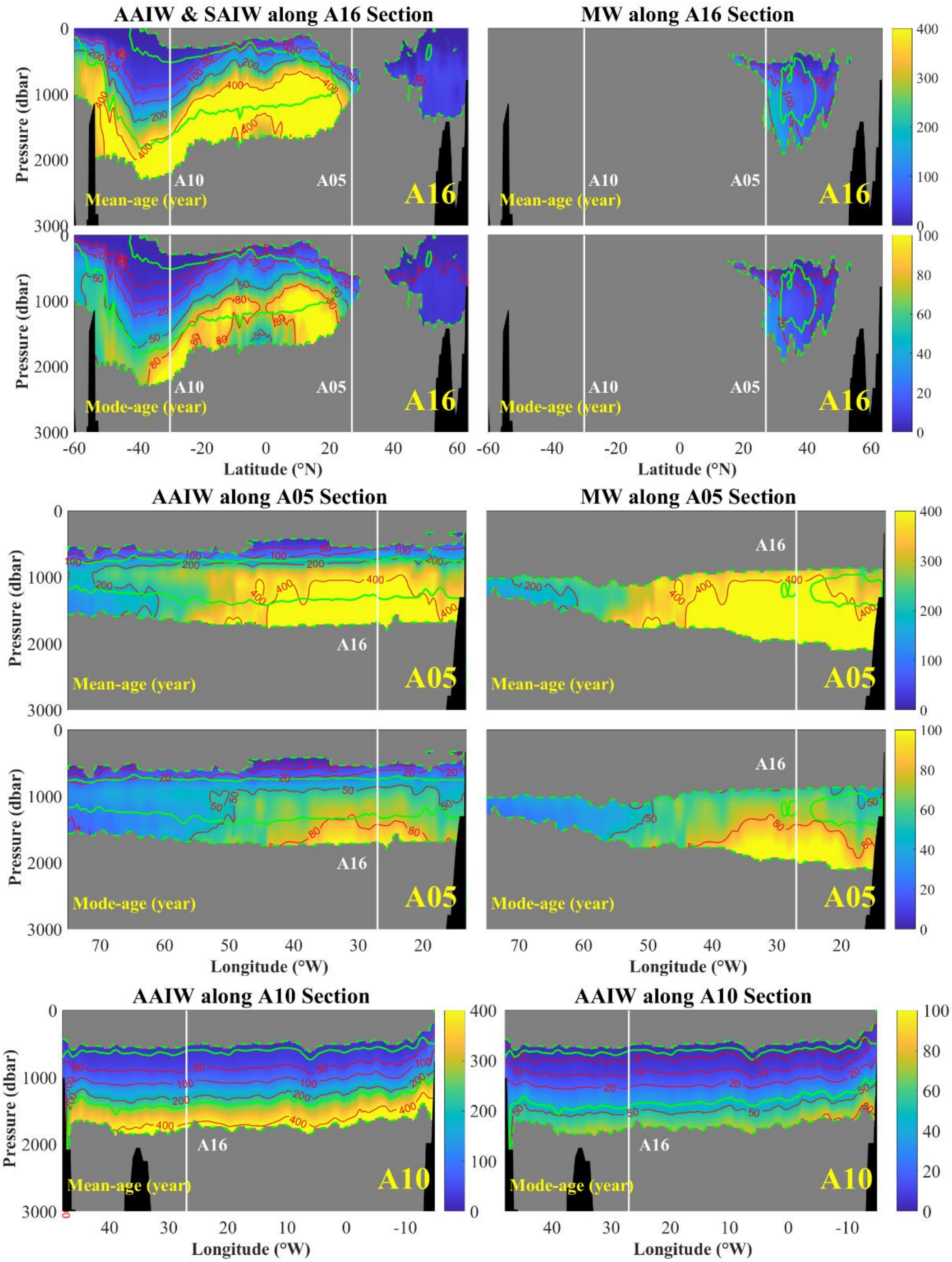

Figure 9. ~~Mean- and m~~Mode-ages of intermediate water masses along the three sections for the upper 4000 dbar. The solid green isolines show the 50% fractions of water masses and the dashed green lines show the 20 % fractions. The grey blank indicates less than 20% contribution from intermediate water mass. White vertical lines show cross overs with other sections.

3.3 Deep and Overflow Layer

The North Atlantic Deep Water (NADW), including its upper and lower portions, dominates the deep and overflow layer (γ between 27.90 and 28.10 kg m^{-3}) of the Atlantic Ocean. This water mass is formed in the high latitude region in the North Atlantic and spreads southward at pressures between 2000 and 4000 dbar until it meets AAIW and AABW in the Antarctic Circum-polar Current (ACC) region. The southward spreading pathway is along the Deep Western Boundary Current (DWBC, Fig. 10, a). Meanwhile, the NADW also extends eastward with the eddies and finally covers the deep and overflow layer (Dickson and Brown, 1994).

Upper and lower North Atlantic Deep Water (NADW): The NADW is a water mass that is transported far southward from its formation area, with a mean-age of ~600 years (Fig. 10, b) and mode-age of ~100 years (Fig. 10, cb) at the southern limb in the Antarctic Circum-polar Current (ACC) region. The increasing ages during the pathway to the south is shown along the A16 section (Fig. 11, a). After leaving the formation area, the mean- and mode-ages increases ~200 and ~20 years respectively from 60 °N to 40 °N. Afterwards, a sharply increase in both ages appear in the region between 30 °N and 10 °N. In this interval, the highest value of mean-age reaches ~1000 years and the mode-age is up to ~150 years. This is because the A16 section at this latitude range passed through the east part of the Atlantic Ocean (east of MAR) and the distance from the Deep Western Boundary Current (DWBC, Fig. 4 and Fig. 10, a) was high. High ages in this region are due to the sluggish water exchange over the ridge. This result can also be confirmed by the observation along the A05 Section (Fig. 11, b): The NADW near the DWBC region has a low mean-age of ~200 years and mode-age of ~40 years, while the ages are up to ~600 years and ~100 years east of the MAR. After passing the equator, when the A16 section returns to the west of the MAR, the mean-ages of NADW are ~400 years and the mode-ages are ~80 years in the latitude range between 0 and 20 °S, which further increase to ~600 (mean-ages) and ~100 (mode-ages) years along the pathway southward until 40 °S. In the ACC region between 40 °S and 60 °S, the mean- and mode-ages of upper and lower NADW decrease to ~400 and ~80 years respectively. Similar to the situation of AAIW in the north Atlantic, this is also the result of mixing with newly formed AAIW and AABW. The spreading of NADW in the zonal direction is slower eastward, so the ages are generally higher in the eastern basin of the Atlantic Ocean (Fig. 10, b and c). The tracer data along the A05 and A10 sections also reflect the above result. In the A05 section, the mean-ages are ~200 years in the west and ~600 or even ~800 years in the east, and the mode-ages show ~50 years in the west and ~100 to ~120 years in the east (Fig. 11, b). In the A10 section, the mean-ages are ~400 years in the west and ~800 years in the east and the mode-ages are ~80 years in the west and ~120 years in the east (Fig. 11, c).

In the vertical direction, the upper NADW mixes with the AAIW from above and the lower NADW mixes with the AABW from below. As the NADW is transported in the opposite direction to these two water masses, the "mixed" ages in the north, which is closer to the formation area of NADW, are higher than the age at the core density of NADW, while the opposite situation exists when spreading to south. After entering the ACC region, both mean-age and mode-age even decreases since the fractions of newly formed AAIW and AABW are high.

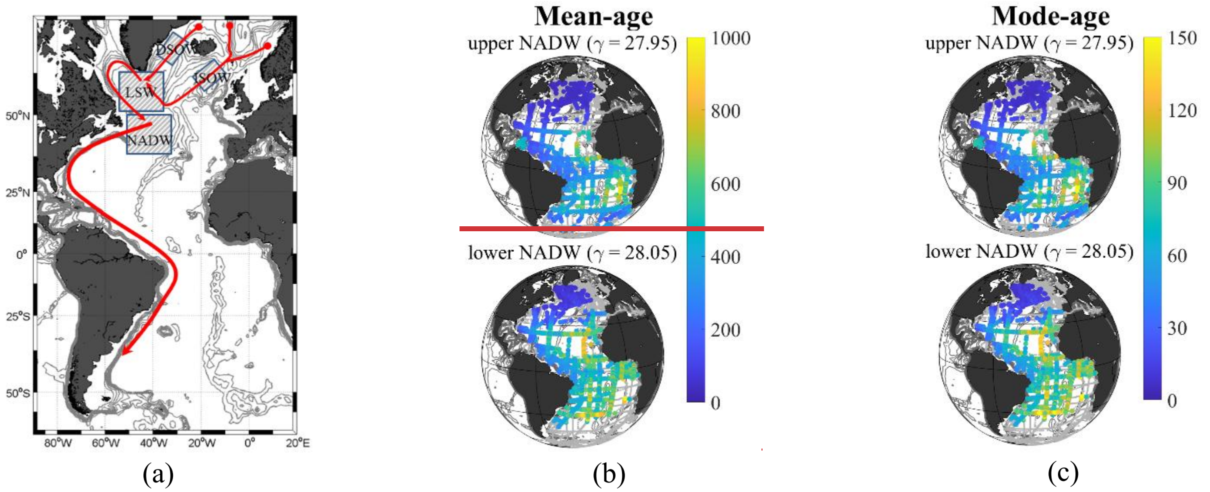

Figure 10. Ages of upper and lower NADW in the Atlantic Ocean.
(a) Main currents in the deep and overflow layer. The currents (arrows) and the formation areas (rectangular shadows) of water masses in the deep and overflow layer.
(b) The ~~mean- and (c)~~ mode-ages of upper and lower NADW at their core neutral densities (kg m^{-3}). The colored dots show the ages in each station. The grey dots show all the GLODAPv2 stations that have less than 20% contribution of the water mass in question or lack of transient-tracer data.

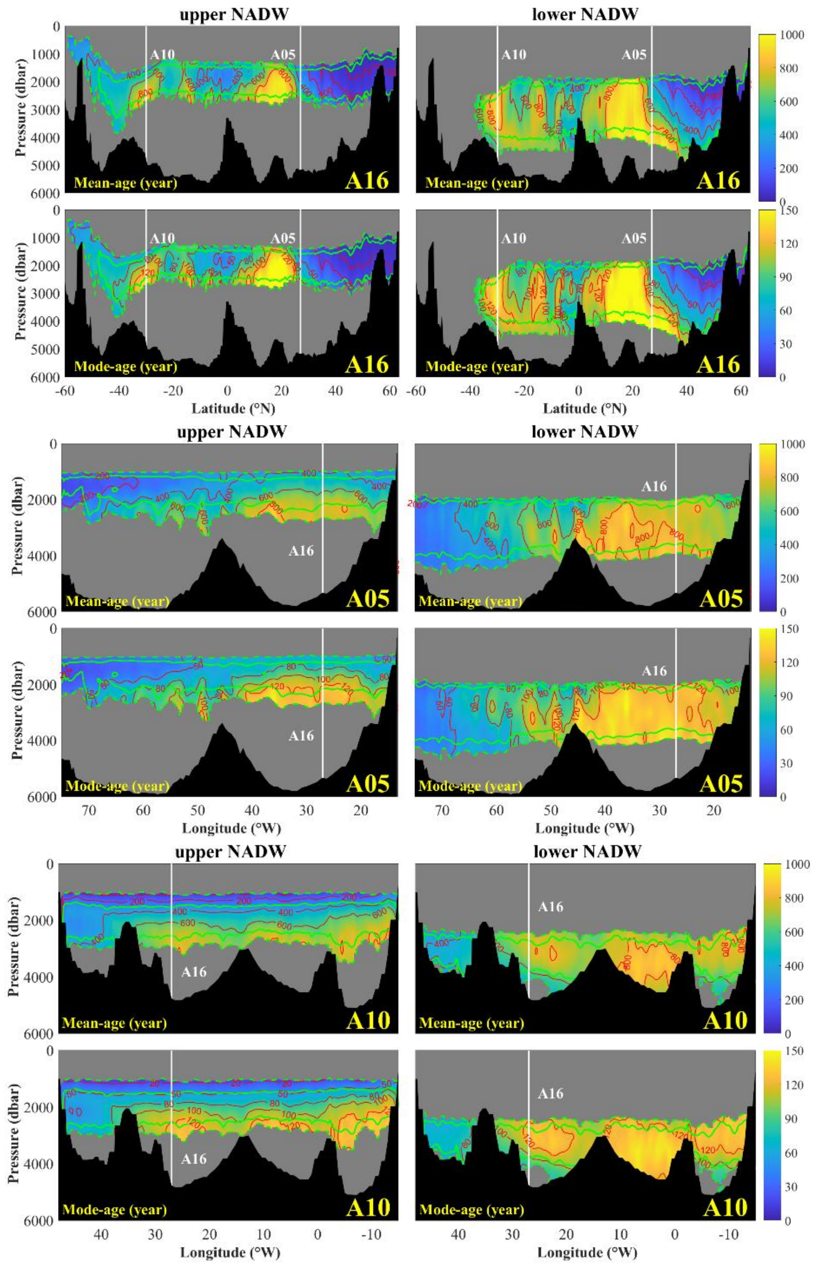

Figure 11. Mean- and mMode ages of upper and lower NADW along the A16 (a), A05 (b) and A10 (c) section lines. The green contour lines show fractions of water masses in 50 % and the dashed green lines show the 20 % fractions. The grey blank indicates less than 20% contribution from NADW. The white vertical lines show cross overs with other section lines.

3.4 Bottom Layer

The bottom layer is noticed already by Wüst, (1933) as it is filled with water from the south. Sverdrup, (1940) further pointed out the role of ACC plays in the formation and spreading of Antarctic Bottom Water (AABW). On this basis, Mantyla and Reid, (1983) elaborated that the most original dense bottom water is restricted near the Antarctic region by topography and the northward flow of bottom water is the mixture of original dense water and the overlying warm water. Gordon and Huber (1990) and Orsi et al., (1999) illustrated that the pathway of AABW to the north is through the Drake Passage sill into the Argentina and Brazilian Basin (Fig. 12, a). In the Atlantic Ocean, the AABW dominates the bottom layer ($\gamma > 28.10$ kg m^{-3}), which origins from the Weddell Sea and spreads to the north. After passing the equator, the AABW is redefined as Northeast Atlantic Bottom Water (NEABW, Liu and Tanhua, 2021).

Antarctic Bottom Water (AABW) & Northeast Atlantic Bottom Water (NEABW): The transport of bottom water is a long process going from the south towards the north. In the meridional direction, the AABW is transported towards the equator with a ~~mean-age of ~600 years and~~ mode-age of ~100 years at the equator, and further northward as NEABW to 40 °N with a ~~mean-age of ~1000 years and~~ mode-age of ~150 years (Fig. 12, b and c). Combined with the A16 Section, more specific segments/details can be seen. In the early stage from the surface of Weddell Sea to the bottom (below the pressure 4000 dbar) at 40 °S, the ~~mean-age of AABW is ~300 years and~~ mode-age is ~50 years. In the range between 10 and 30 °S, high values of ~~~800 years (mean-age) and~~ ~120 years (mode-age) appear due to the mixing with the lower NADW with high ages (Fig. 13, a). After passing the equator, the redefined NEABW contains a ~~mean-age up to ~1000 years and~~ mode-age up to ~150 years at 40 °N, indicating that the bottom water, including the AABW and NEABW, takes about 150 years (mode-age) for the transport from the formation area (Weddell Sea) to 40 °N. North of 40 °N, the ages decrease due to the mixing with newly formed lower NADW in this region (Fig. 12, b and c, Fig. 13, a). The distribution of mean- and mode-ages also show a difference in the zonal direction. As shown in Fig.12 b and c, the general age distribution presents a trend with lower ages in the west, and higher in the east. Along the A10 section at 30 °S, the AABW has a mean-age of ~400 in the west and ~600 years in the east, whereas the mode-age is ~50 in the west and ~100 in the east. A similar situation is recorded along the A05 section; the mean-age of NEABW is ~600 years in the west and ~800 years in the east, whereas the mode-age is ~80 years in the west and between ~120 years in the east (Fig. 13, b). An additional factor that affects the age distributions is the mixing between AABW and NADW. In the south hemisphere, both ages are relatively low (~400 years for mean-age and ~80 years for mode-age) at the pressures below 4000 dbar, where the AABW has a fraction higher than 50%, while the ages are significantly higher when the AABW mixes with lower NADW at pressure of ~3000 dbar, especially in the region between 0 and 10 °W, the mean-age reaches up to ~800 years and the mode-age is ~120 years. This is because the "old" NADW takes up a fraction for more than 50% to 80%. The situation in the north hemisphere is the opposite, the ages of NEABW are higher in the bottom layer below 4000 dbar but lower in the deep layer at 3000 dbar due to the mixing with the young NADW. In the western basin, the mean-age is ~ 600 years and mode-age is ~80 years in the bottom, while ~400 years and ~50 years when mixes with NADW. Similar in the east basin, the mean-age is ~800 years and mode-age is ~120 years below 4000 dbar, while ~600 years and ~100 years at 3000 dbar (Fig. 13, b).

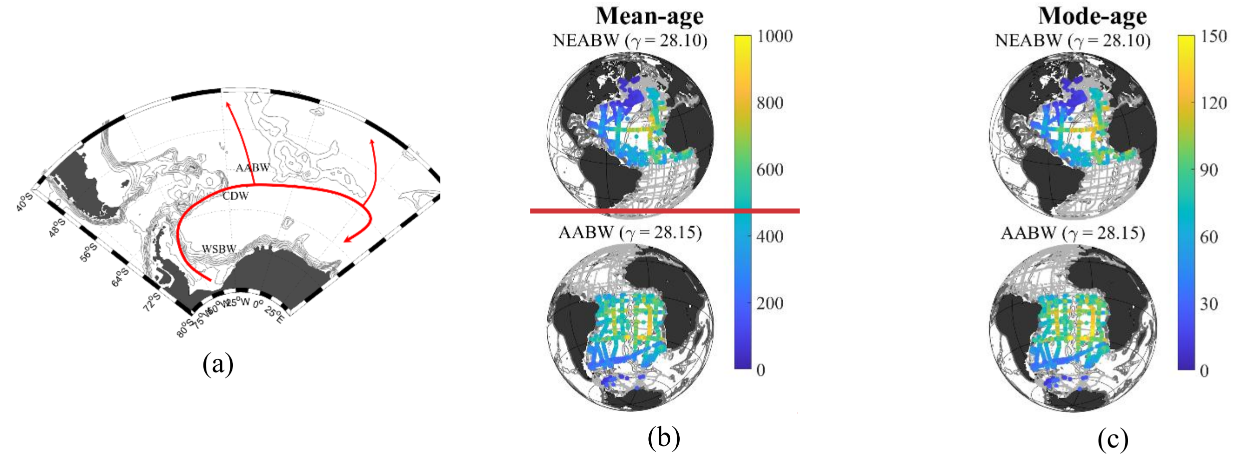

Figure 12. Ages of bottom water masses in the Atlantic Ocean.
(a) Main currents in the bottom layer. The currents (arrows) and the formation areas (rectangular shadows) of water masses in the deep and overflow layer.
(b) The ~~mean- and (c) m~~Mode-ages of bottom water masses at their core neutral densities (kg m^{-3}). The colored dots show the ages in each station. The grey dots show all the GLODAPv2 stations that have less than 20% contribution of the water mass in question or lack of transient-tracer data.

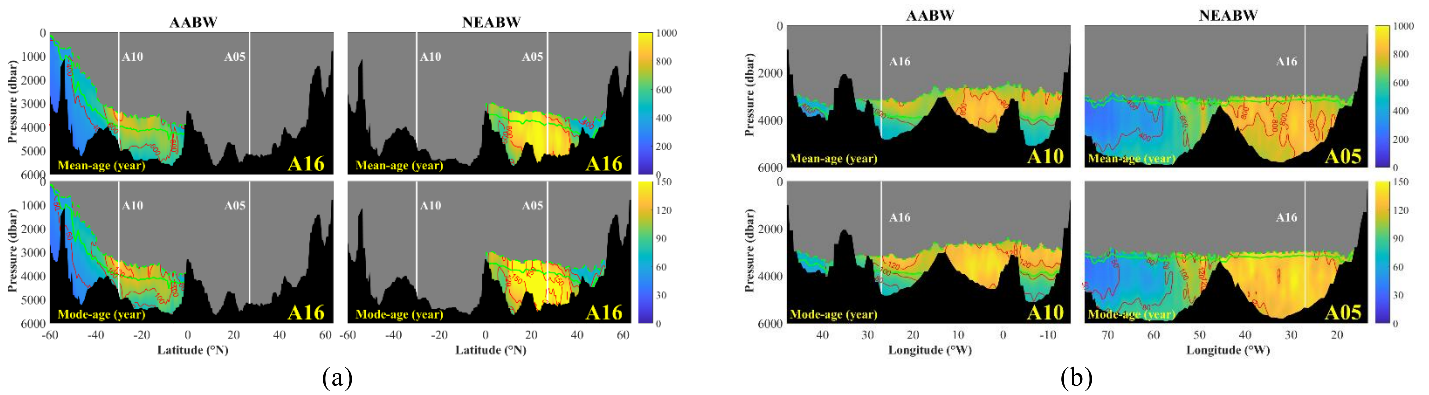

Figure 13. M<u>ode</u>~~ean~~-ages of AABW and NEABW along the A16 (a), A05 and A10 (b) section lines. The green contour lines show fractions of water masses in 50 and the dashed green lines show the 20 % fractions. The grey blank indicates less than 20% contribution from bottom water masses. The white vertical lines show cross overs with other section lines.

4 The application of water mass ages in estimating the oxygen utilization rate (OUR)

The transit time distribution (TTD) provides a framework for using transient tracers to estimate the time scales governing ventilation, which in turn can be applied to quantify biogeochemical rates. For instance, based on the TTD determined from the tracer observations, Wang et al., (2021) estimated the OUR in the northern South China Sea.

The oxygen concentration in seawater under steady state is maintained by the balance of supply from oxygen-rich surface water and consumption by the respiration of organic matter. The Apparent Oxygen Utilization (AOU) shows the accumulated oxygen consumption in a water mass since isolated from the atmosphere, and is defined as the difference between saturated and measured oxygen concentration (i.e. AOU = $Oxy_{saturated}$ - $Oxy_{measured}$, Redfield, 1942; Redfield et al., 1963; Pytkowicz, 1971). The Oxygen Utilization Rate OUR (μmol kg^{-1} yr^{-1}) can be calculated from AOU and water mass age and shows the integrated oxygen utilization rate (oxidation rate) during the pathway of a water mass from surface of the formation area to the sampling location (Jenkins, 1987; Doney and Bullister, 1992; Sonnerup et al., 2013). In addition, the OUR is also an important indicator in characterizing the combination of ventilation and respiration of the interior ocean (Koeve and Kähler, 2016; Thomas et al., 2020).

The true, or local OUR is difficult to estimate, and the main difficulty focuses on the determination of the "true" water mass age since the seawater comes from different pathways due to the mixing in the ocean interior (Tomczak, 1999; Koeve and Kähler, 2016). Researchers have tried a variety of ways to define the age of a water mass. For instance, the tracer-age (CFC age) is used in Karstensen et al., (2008), while the mean-age (partial pressure ages) is used in Sonnerup et al., (2015) in estimating the "integrated" water mass age that effects the oxygen consumption. As described in Section 2.2, the mean-age represents the average of all the parts in one water sample, so the OUR calculated from mean-age is a "mixed" value of all the contributing water masses in the sample. In the steady state, the mean-age can reflect the "mixed" or "integrated" OUR objectively. The OUR is not constant over the life-time of a water mass, but is strongly depth and temperature dependent. Neither using the mode-age or the mean-age will be a reflection of the local OUR. The mean-age (Γ) represents the average time elapsed since all water parcels in the sample were last in contact with the atmosphere, integrating over all pathways including long tails of older water, that most often has seen very low OUR in the interior ocean. In contrast, the mode-age, representing the most probable transit time, better captures the advective timescale of the dominant water mass along its dominant pathway from its formation region. The OUR calculated from mode-ages thus more closely approximates the time available for respiration to occur along the core of the water mass's trajectory. Using the mean-age, which includes much older water fractions will yield unrealistically low rates. We choose to use mode-age since it provides values in approximately the right magnitude, noting again that this value is not an absolute measure of local OUR.

Water masses with mode-ages larger than ~50 years in some parts of their distribution, including the AAIW, NADW, AABW and NEABW in the Atlantic Ocean, are defined here as wide-spread water masses. The transports of these wide-spread water masses are significantly influenced by the currents and topography. Therefore, their mode-age shows regional differences. Such differences also exist in DO and AOU, and lead to the spatial differences in OUR, especially between the eastern and western basins (Fig. 14). In the meridional direction, the mode-age increases with the distance from formation area. In the zonal direction, significant differences exist between the east and west of MAR. The wide-spread water masses generally have lower mode-ages in the western basin, which is better ventilated by the WBC and the DWBC (Fig. 14, left). In addition, surface oxygen-rich water is transported by these water masses to the deeper layers and are gradually consumed during the path-way. As a result, the DO is highest in the formation area and decreases with the distance. Meanwhile, the western basin displays higher DO due to the better ventilation (Fig. 14, middle left). The OUR shows a similar distribution to DO indicating that higher oxygen consumption rate, or oxidation rate is co-located with the regions with high oxygen concentration. At the same time, Fig. 14 also shows that the OUR approaches 0 when the mode-age is larger than ~50 years.

In the intermediate layer, the AAIW show low mode-ages, high DO and low AOU in the formation area near the Antarctic region. During the northward transport between 40 °S and 20 °N, the mode-ages increase and the DOs decrease with distance from the formation area (Fig. 14, upper panel). In general, the mode-ages are lower in the west, while the zonal difference for DOs are not significant except for some regions in the eastern basins. The mode-ages are mostly between ~60 and ~90 years and reaches up to ~120 years in the poor ventilated eastern basin. The DOs are between 160 and 220 μmol kg^{-1} in the south hemisphere and mostly between 100 and 160 μmol kg-1 in the north hemisphere. The OURs in the Antarctic region obtain the highest value in the latitude region between 20 and 40 °S and decrease on the pathway to the north until 20 °N.

In the deep and overflow layer, the NADW is newly formed in the high north latitude. In most regions covered by the NADW between 30 °N and 40 °S, the differences between west and east exist with obvious low mode-age and AOU (high DO) and in the west, where is well ventilated by the DWBC (Fig. 14). The mode-age is between ~30 and ~60 years in the west and between ~90 and ~150 years in the east. The AOU is lower in the west and higher in the east. The OUR, which shows the opposite distribution as the AOU in the zonal direction, obtains the highest value in the formation area of NADW, maintains relative higher in the west along the DWBC region and shows a lower value in the eastern basin.

The bottom layer is occupied by the AABW and NEABW in the south and north hemisphere respectively. The AABW is formed in the Antarctic region with an original mode-age lower than ~30 years and increases on the way to the north. Similar to the AAIW and NADW, the western basin is better ventilated, therefore the mode-ages are lower in the west at the same latitude (Fig. 14, lower panel). In contrast to the AAIW and NADW, the AABW obtains relative lower DOs and higher AOUs when formed (see also Fig. 15, b). In the western basin of the South Atlantic, the DOs decrease to 220 μmol kg^{-1} and the AOUs increase to 130 μmol kg^{-1} on the pathway, while in the eastern basin, the DOs are 240 μmol kg^{-1} and the AOUs are 110 μmol kg^{-1}. This is because the eastern basin is more influenced by the relative oxygen-rich NADW from the north. Similarly, the DOs and AOUs of NEABW in the North Atlantic also show similar states to the NADW. In west regions ventilated by the DWBC, the DOs reach the values of higher than 260 μmol kg^{-1} and AOU is lower than 70 μmol kg^{-1}. This result can also be confirmed in Figure 15. Although the distributions of DOs and AOUs are more complex in the bottom layer, the OURs still match the distribution of mode-ages. The highest OURs appears in the formation area near the Antarctic region with values higher than 4 μmol kg^{-1} yr^{-1}. In the western Atlantic region with low mode-ages, the OURs show relative higher values (> between 1 and 3 μmol kg^{-1} yr^{-1}) and low value (below 1 μmol kg^{-1} yr^{-1}) in the east (Fig. 14, lower panel).

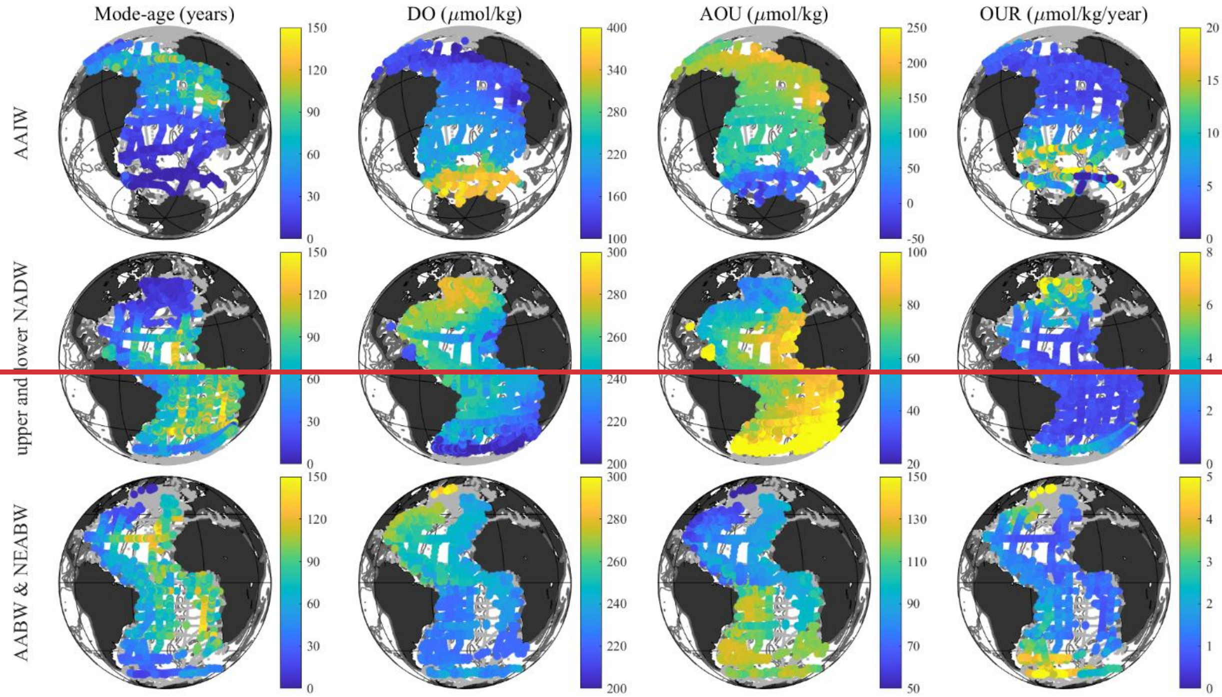

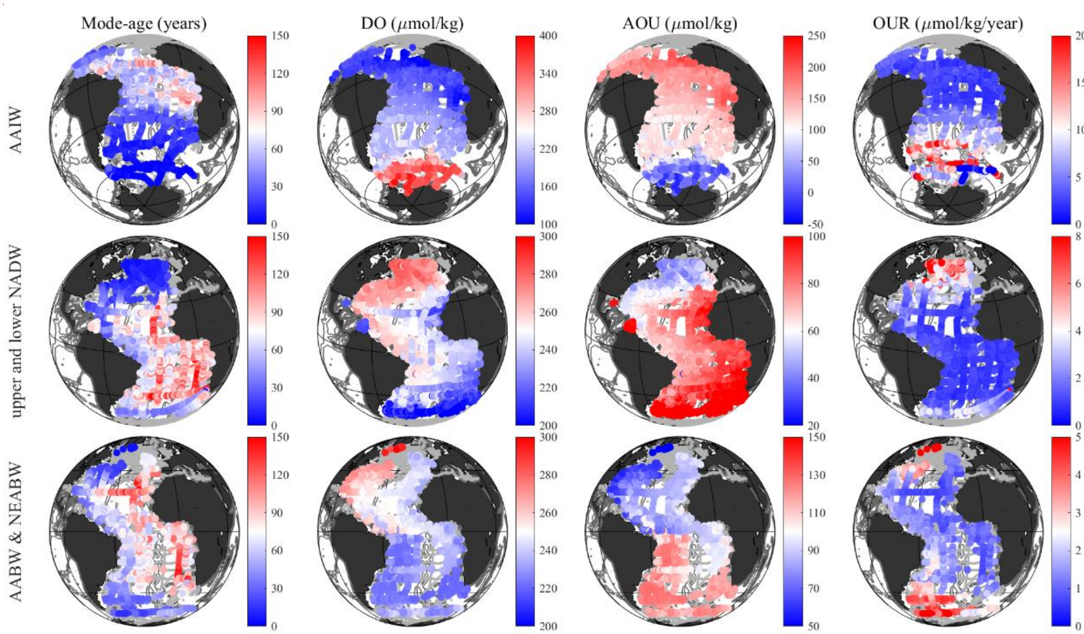

Figure 14. Mode-age, DO, AOU and OUR of wide-spread water masses in the Atlantic Ocean. The colored dots show the values in each station at core neutral densities of each water mass (AAIW at 27.20, upper NADW at 27.95, lower NADW at 28.05, AABW at 28.15, NEABW at 28.10 kg m^{-3}, the upper and lower NADW, AABW and NEABW are shown in one plot. The grey dots show all the GLODAPv2 stations that have less than 20%

contribution of the water mass in question. Note: Negative AOU values indicate oxygen supersaturation, which is typically observed in well-ventilated surface or near-surface waters.

The above four properties are also represented along the A16 section (Fig. 15). The AAIW has the lowest mode-age among the three water masses, but also the largest variations in the DO and AOU. The mode-age indicates that in total of ~40 to 60 years is needed for the main body of AAIW (fractions > 80%) to be transported to the equator (Fig 15, a). The DO decreases rapidly from 260 to below 180 μmol kg^{-1} at the oxygen minimum zone at 20 °S, while the AOU increases from 60 to 150 μmol kg^{-1} during the northward pathway (Fig 15, b and c). The OUR is higher than 8 μmol kg^{-1} yr^{-1} at the beginning and decreases to 3 μmol kg^{-1} yr^{-1} close to the equator (Fig 15, d). The mode-age of NADW is ~140 years at 40 °S and reaches a peak of ~160 years in the region of 20 °N due to the sluggish water exchange caused by the topography. The NADW contains the highest oxygen concentration and the lowest AOU and OUR in the abyssal Atlantic Ocean. The value of DO is 260 μmol kg^{-1} at the starting point at 60 °N and still remains 220 μmol kg^{-1} at 40 °S where it meets the AABW and AAIW. The AOU of NADW remains below 100 μmol kg^{-1} during the entire pathway. The OUR of NADW is below 5 μmol kg^{-1} yr^{-1} close to the formation area, and below 1 μmol kg^{-1} yr^{-1} south of 60 °N. The transport of the main body of AABW takes in total of ~100 years from the Weddell Sea to the equator. The DO and AOU remain unchanged at 220 and 130 μmol kg^{-1} respectively on the pathway to the equator, indicating very low OUR. Although derived from the AABW, the characteristics of the NEABW are more similar to the NADW in all the above properties.

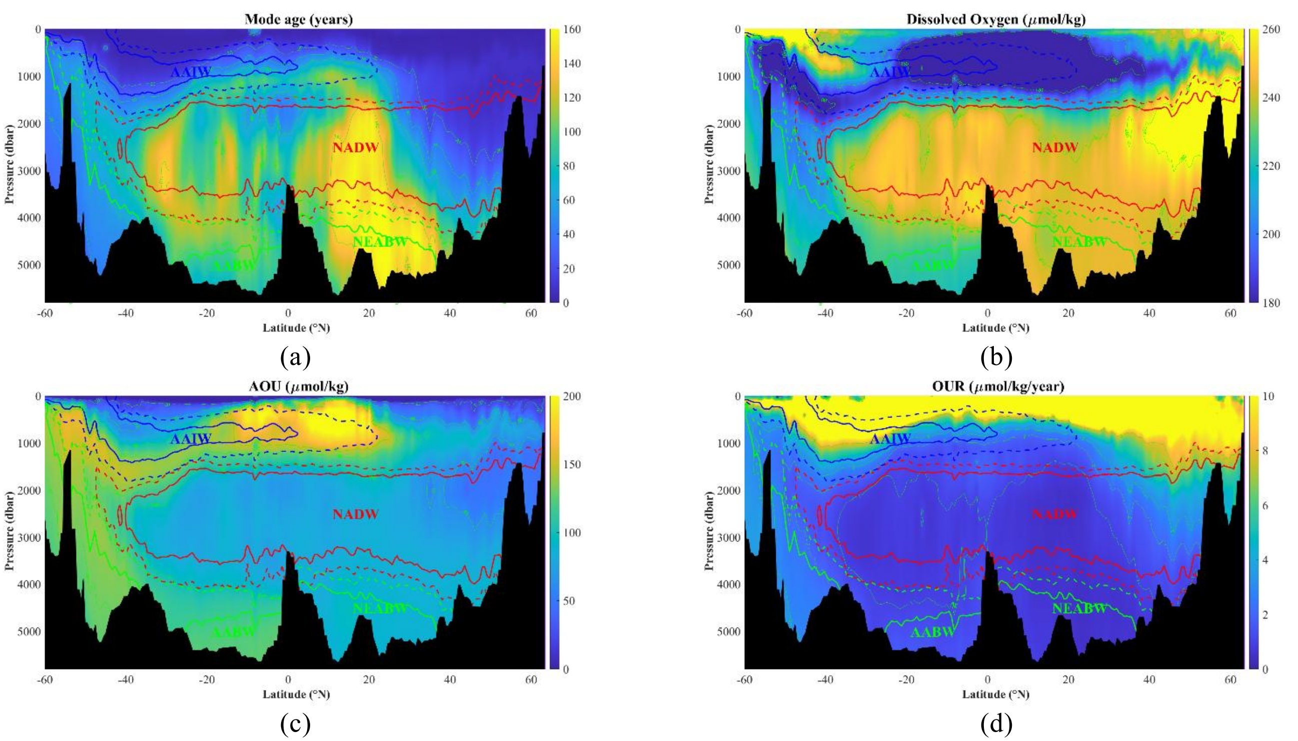

Figure 15. Distributions of (a) mode-age, (b) dissolved oxygen, (c) AOU and (d) OUR along the A16 section line. The color solid lines show the fractions of 80% in each water mass and the dashed lines show the fractions of 50%.

5 Estimation of water mass ages based on ^{39}Ar

As a representative of noble gas radionuclides, ^{39}Ar is considered to exhibit nearly ideal chemical and physical properties for studying earth and environmental processes (Lu et al., 2014). In this study, the mean- and mode- ages of Atlantic wide-spread water masses, including AAIW, NADW, AABW, and NEABW, are also estimated based on observations of ^{39}Ar. For this purpose, we make a distinction between the western (green dots) and eastern (red dots) Atlantic, divided by the Mid-Atlantic-Ridge (Fig. 16a). The distribution of ^{39}Ar is shown in Fig. 16 b. Near the formation area of each wide-spread water mass, the concentration of ^{39}Ar approaches approximately 100%, indicating that the surface waters are in equilibrium with the atmosphere. As these water masses are transported over long distances and extended periods, the continuous decay of ^{39}Ar leads to concentrations decreasing to roughly 30% at their furthest locations. By integrating this information with its half-life of 269 years, the water mass ages can be estimated. For ^{39}Ar we focus our attention to the older water masses, as the younger ones are better characterized by CFC12 and SF_6.

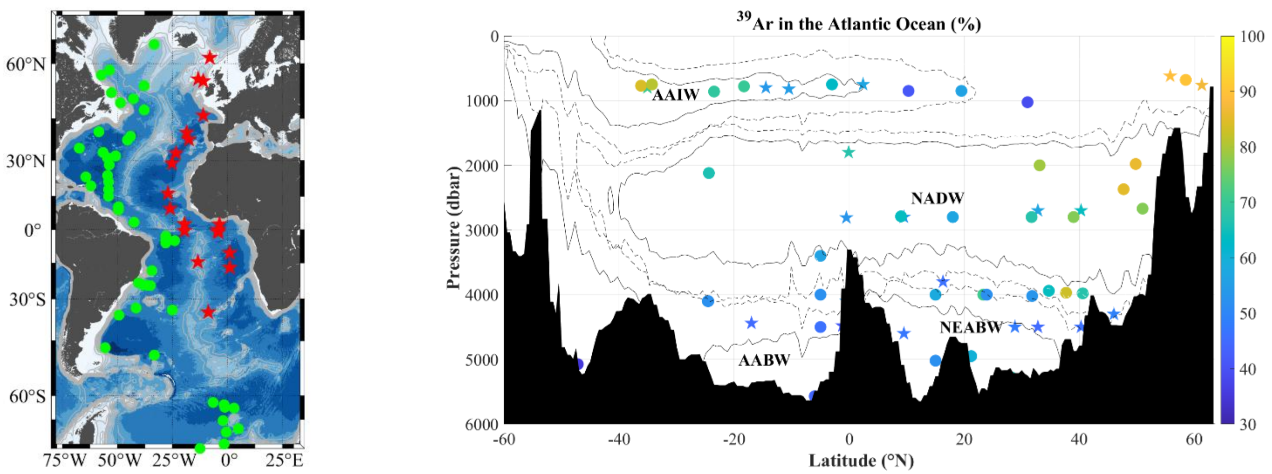

(a) (b)

Figure 16. (a) Map of the ^{39}Ar sampling stations. The green circle dots show the stations in the west Atlantic Ocean (west of M-A-R), while the red stars show the stations in the east Atlantic Ocean. (b) Distributions of ^{39}Ar in the Atlantic Ocean (% Modern). The circle dots show the data in the west, while the stars show the data in the east Atlantic Ocean. The solid isolines show the 80% fractions of water masses and the dashed lines show the 50% fractions.

Similar to the findings from CFC-12 and SF_6 observations, the mean- and mode-ages derived from measurements using ^{39}Ar increase with transport from the source of formation (Fig. 17). At a latitude of approximately 40°S, the AAIW exhibits mean-ages ranging between ~100 to ~200 years (with mode-age around ~30 years). When transported northward to about 20°S, both mean- and mode-ages rise to roughly ~300 years and ~60 years respectively. Upon reaching approximately 10°N during further northward transport, these values escalate to around ~700 years for mean-age and ~100 years for mode-age. However, near the region at about 20°N, the terminus for northward flow, the mean-age decreases back down to roughly ~400 years while maintaining a mode-age close to ~60 years due to mixing with younger upper NADW. In the deep and overflow layer, the newly formed NADW initiates at high northern latitudes, exhibiting both mean- and mode-ages approaching zero. During southward transport at around 30 °S, the concentration data indicates corresponding mean- and mode-ages of approximately ~400 years and ~60 years respectively. Similarly, the bottom water masses (AABW and NEABW) display mean- and mode-ages of around ~500 years and ~100 years respectively at the farthest end of the transport distance approximately 50 °N.

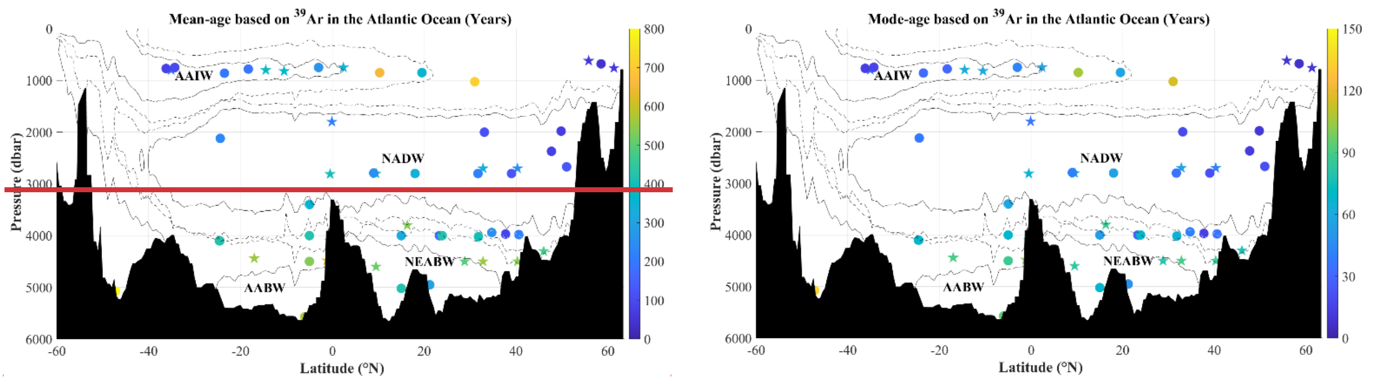

(a) ~~(b)~~

Figure 17. ~~Mean- (a) and m~~Mode-ages ~~(b)~~ of the wide-spread water masses estimated by ^{39}Ar in the Atlantic Ocean. The circle dots show the data in the west, while the stars show the data in the east Atlantic Ocean. The solid isolines show the 80% fractions of water masses and the dashed lines show the 50 % fractions.

The contrast between the western and eastern Atlantic Ocean is distinctly evident (Fig. 16, b). Generally, higher concentrations of ^{39}Ar are observed in the west compared to the east at equivalent latitudes. For instance, in the vicinity of the AAIW formation area at 40 °S, the ^{39}Ar concentration is approximately 100% in the west and around 70% in the east. In the intermediate layer near the equator, these concentrations decrease to about 70% (west) and 50% (east). These findings suggest that both mean- and mode-ages of AAIW are close to zero at 40 °S. The mean-age is estimated to be ~300 years in the west and ~500 years in the east north of 40°S. Similar results are also observed in the deep water and overflow layers. Based on elevated levels of ^{39}Ar near its formation area, it can be inferred that both mean- and mode-ages of NADW are close to zero at 60 °N across both West and East Atlantic Oceans. Between 20 °N and the equator, the mean-age is estimated to be ~300 years in the west and ~500 years in the east; while the mode-age is around ~60 years (west) and ~90 years (east), respectively. For bottom water masses below a depth of 4000 m, concentrations of ^{39}Ar generally fall below 50%, with higher levels observed in the west (50%-60%) compared to lower levels seen in the east (40%-50%) between 20 °S and 40 °N, indicating the water mass ages range from ~400–500 years (mean-age) and ~60–90 years (mode-age) in the west, and from ~500–600 years (mean-age) and ~90–120 years (mode-age) in the east.

Table 2: Comparison of water mass ages (mean- and mode-age) estimated from CFC-12/SF_6 and ^{39}Ar

Uncertainties for CFC-12/SF_6 are derived from mixing ratio sensitivity tests ($\Delta/\Gamma = 0.8 - 1.2$); uncertainties for ^{39}Ar are from measurement statistics (1σ). Location definitions: "West" = west of Mid-Atlantic Ridge (MAR); "East" = east of MAR.

Water Masses	Age Type (years)	Tracer	Location	Latitude/Longitude Range	Neutral Density (kg m^{-3})	Age ± Uncertainty (years)
AAIW	Mean-age	CFC-12 & SF_6	West	35–45 °S, 60–20 °W	27.15–27.25	70 ± 10
			East	35–45 °S, 20 °W–10 °E	27.15–27.25	200 ± 25
		^{39}Ar	West	35–45 °S, 60–20 °W	27.15–27.25	150 ± 20
			East	35–45 °S, 20 °W–10 °E	27.15–27.25	175 ± 20
		CFC-12 & SF_6	West	15–25 °S, 40–20 °W	27.20–27.30	300 ± 35
			East	15–25°S, 20 °W–10 °E	27.20–27.30	500 ± 60
		^{39}Ar	West	15–25 °S, 40–20 °W	27.20–27.30	300 ± 40
			East	15–25 °S, 20 °W–10 °E	27.20–27.30	500 ± 60
	Mode-age	CFC-12 & SF_6	West	35–45 °S, 60–20 °W	27.15–27.25	10 ± 2
			East	35–45 °S, 20 °W–10 °E	27.15–27.25	30 ± 4
		^{39}Ar	West	35–45°S, 60–20°W	27.15–27.25	30 ± 5
			East	35–45 °S, 20 °W–10 °E	27.15–27.25	35 ± 5
		CFC-12 & SF_6	West	15–25 °S, 40–20 °W	27.20–27.30	50 ± 8
			East	15–25°S, 20°W–10°E	27.20–27.30	80 ± 12
		^{39}Ar	West	15–25 °S, 40–20 °W	27.20–27.30	60 ± 10
			East	15–25 °S, 20 °W–10 °E	27.20–27.30	90 ± 15
NADW	Mean-age	CFC-12 & SF_6	West (A05)	15–25 °N, 70–40 °W	27.95–28.05	200 ± 30
			East (A05)	15–25°N, 40–10°W	27.95–28.05	600 ± 80
		^{39}Ar	West	15–25 °N, 70–40 °W	27.95–28.05	130 ± 20
			East	15–25 °N, 40–10 °W	27.95–28.05	400 ± 50

	Mode-age	CFC-12 & SF_6	West (A05)	15–25 °N, 70–40 °W	27.95–28.05	40 ± 6
			East (A05)	15–25 °N, 40–10 °W	27.95–28.05	100 ± 15
		^{39}Ar	West	15–25 °N, 70–40 °W	27.95–28.05	40 ± 6
			East	15–25 °N, 40–10 °W	27.95–28.05	80 ± 12
AABW & NEABW	Mean-age	CFC-12 & SF_6	West (A10)	25–35 °S, 50–30 °W	>28.10	400 ± 50
			East (A10)	25–35 °S, 10 °W–10 °E	>28.10	600 ± 80
		^{39}Ar	West	25–35 °S, 50–30 °W	>28.10	500 ± 60
			East	25–35 °S, 10 °W–10 °E	>28.10	600 ± 70
	Mode-age	CFC-12 & SF_6	West (A10)	25–35 °S, 50–30 °W	>28.10	50 ± 8
			East (A10)	25–35 °S, 10 °W–10 °E	>28.10	100 ± 15
		^{39}Ar	West	25–35 °S, 50–30 °W	>28.10	90 ± 12
			East	25–35 °S, 10 °W–10 °E	>28.10	110 ± 15

Notes: The ages are core values at the specified neutral density ranges. For NADW, "A05" refers to the zonal section at ~24 °N; for AABW/NEABW, "A10" refers to the zonal section at ~30 °S. Uncertainty ranges are rounded to nearest 5 years. ^{39}Ar data are from stations not exactly coincident with CFC-12/SF_6 stations; spatial pairing criteria are described in Section 5 and Fig. 18.

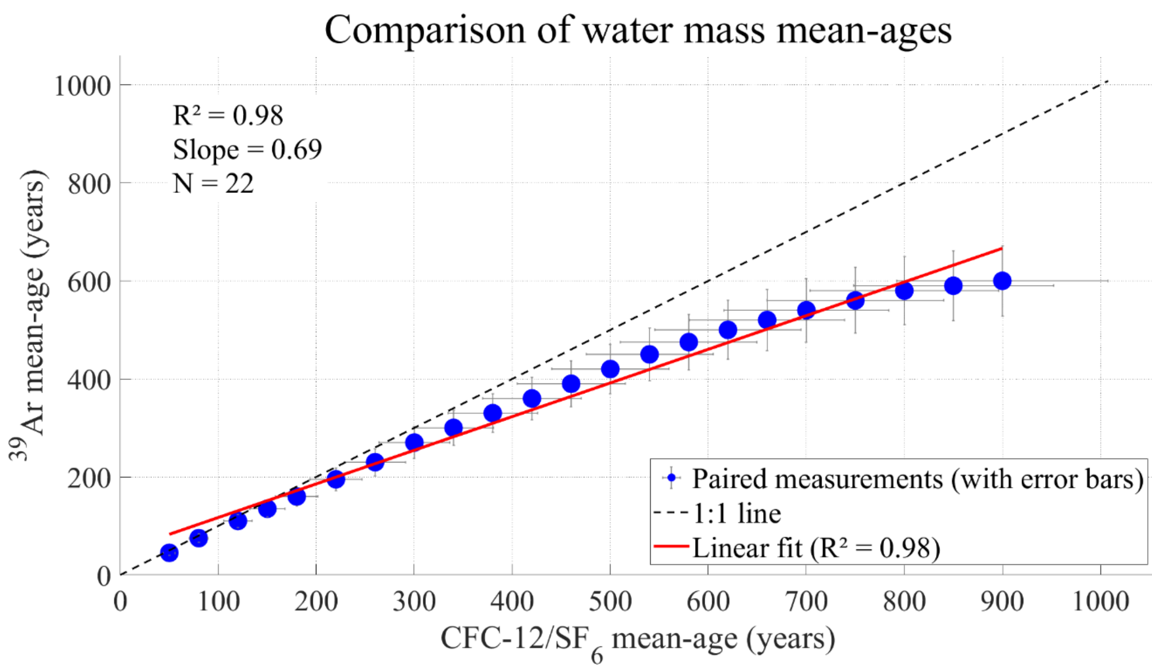

Figure 18. Paired comparison of mean ages from CFC-12/SF_6 vs. ^{39}Ar Error bars as defined in text. Linear regression yields $R^2 = 0.98$ ($N = 22$). Systematic overestimation by CFC-12/SF_6 for ages >300 years is evident, while both methods agree for younger waters. The high R^2 confirms overall consistency, and the offset demonstrates the advantage of ^{39}Ar for old water masses.

To provide a more quantitative comparison, we paired each ^{39}Ar measurement with the nearest CFC-12/SF_6-derived mean-age from GLODAPv2 (within 2° in latitude/longitude and 200 dbar in pressure). The resulting scatter plot (Fig. 18) shows a positive correlation ($R^2 = 0.67$) but with a systematic deviation from the 1:1 line: for ages > 300 years, CFC-12/SF_6 ages are consistently higher than ^{39}Ar ages by 150–300 years, while for ages < 300 years the two estimates agree within uncertainties. This supports our earlier conclusion that CFC-12/SF_6 may overestimate ages in deep, old waters due to concentrations near detection limits, whereas ^{39}Ar provides more reliable ages on centennial to millennial timescales.

As expected, the inferred ages of water masses differ depending on the tracer employed. These discrepancies arise not only from potential limitations in the assumed IG-TTD, but also from the distinct temporal validity ranges and detection limits of each tracer. Our comparative analysis (as summarized in Table 2 and Fig. 18) reveals a systematic pattern: mean- and mode-ages derived from ^{39}Ar are generally lower than those estimated from CFC-12 and SF_6 for deeper/older water masses. This is exemplified by the NADW in the eastern basin near 20°N, where CFC-12/SF_6 yield a mean-age of ~1000 years and a mode-age of ~150 years, whereas ^{39}Ar suggests younger ages of ~600 and ~90 years, respectively. Similarly, for AABW/NEABW near 50 °N, CFC-12 and SF_6 based estimates (~800 years mean, ~120 years mode) exceed those from ^{39}Ar (~500 years mean,

~100 years mode). A likely explanation for this systematic tendency towards higher age estimates from CFC-12 and SF_6 in deep and bottom layers might be attributed to their extremely low concentrations at great depths and for older waters. These concentrations often approach or fall below analytical detection limits, which can amplify uncertainties and appear to skew age calculations towards higher values. In contrast, the ^{39}Ar with 269-year half-life appears to be better suited for dating waters with transit times on the order of centuries to a millennium, and thus could provide relative more robust age estimates for these older water masses, as its slower decay rate remains measurable over such longer timescales.

Figure 18 shows a scatter plot of ^{39}Ar-derived mean ages versus CFC-12/SF_6-derived mean ages for collocated stations (within 2° latitude/longitude and 200 dbar). The positive correlation ($R^2 = 0.98$) confirms the qualitative consistency between the two tracer approaches. However, systematic deviation from the 1:1 line is evident: for ages exceeding 300 years, CFC-12/SF_6 ages are consistently higher than ^{39}Ar ages by approximately 150–300 years, while for younger waters the two estimates agree within uncertainties. This supports the interpretation that CFC-12 and SF_6 approach detection limits in deep, old water masses, leading to overestimation, whereas ^{39}Ar provides more reliable ages on centennial to millennial timescales.

6 Conclusions and discussion

The geographic distributions of main water masses in the Atlantic Ocean are reported in Liu and Tanhua (2021). In the present work, the transports of water masses are traced by transient tracers (CFC-12, SF_6 and ^{39}Ar) and their ventilation timescales (water mass ages) are quantified. Three distinct concepts of water mass age are discussed within the analytical framework. While the tracer-age concept (assuming purely advective transport) is introduced for context, the quantitative analysis and results presented herein are based on the mean-age and mode-age derived from the Transit Time Distribution (TTD) model. The application of a standard mixing ratio ($\Delta/\Gamma = 1$) and 100% surface saturation is followed. The mean-age, representing the average transit time of all water parcels in a sample and providing an integrative timescale, is used to characterize the overall ventilation status. The mode-age, representing the most probable transit time and serving as a proxy for advective timescales, is applied to trace the dominant transport pathways and to estimate process rates like the oxygen utilization rate (OUR).

In general, the water mass age increases with the depth and distance from the formation area, so the central waters in the upper layer obtain the lowest ages of within ~100 years. In the intermediate layer, the AAIW and MW are two conspicuous water masses and both take ~300 years to spread from south to north (AAIW) and east to west (MW) respectively. As the dominant water mass in the deep and overflow layer, the NADW takes ~500 years to spread along the DWBC in the west Atlantic Ocean, and takes ~ 900 years eastward to cover the east part. The bottom waters origin from south of Antarctic Circumpolar Current region take ~600 years to spread northward and cover the bottom layer. Similar as the NADW, the mean-age of both AABW and NEABW show spatial difference between the west (low mean-age) and the east (high mean-age). This is because the west Atlantic Ocean is well ventilated by the DWBC while the water exchange is sluggish in the east.

The transient tracers (CFC-12, SF_6 and ^{39}Ar), serve as effective tools for identifying and quantifying oceanographic ventilation, each tracer possessing distinct advantages and limitations in determining and tracing the depths and mean ages of water masses. CFC-12 and SF_6 exhibit optimal applicability for water masses range within 2000 dbar pressure (or mean-ages < ~500 years). However, their utility becomes constrained in deeper aqueous regimes (below 2000 dbar or mean-age > ~500 years) due to inherent limitations in tracer concentration sensitivity, which may induce systematic overestimations of water mass ages when applied to deep or bottom layers. The chemically inert radioisotope ^{39}Ar, characterized by a 269-year half-life, effectively addresses this observational gap through its unique temporal resolution. Consequently, the synergistic application of SF_6, CFCs, and ^{39}Ar in multi-tracer frameworks overcomes temporal constraints inherent to single-tracer approaches, enabling comprehensive investigation of coupled biogeochemical-climate interactions. This integrated methodology facilitates novel insights into climate-driven water mass reorganization, carbon cycle dynamics, and other critical marine processes essential for understanding oceanic responses to global change.

The ventilations and respiration rates (oxidation rates, OUR) of wide-spread water masses are estimated by the mode-ages. The currents and topography have significant impacts on the mode-ages and furthermore the the apparent oxygen utilisation rate (OUR). The western basins of the Atlantic Ocean are better ventilated with lower the mode-ages, while the OURs show the opposite distribution, suggesting that the mode-age is an important determinant of OUR in seawater than AOU and higher respiration rates exist when the region is better ventilated.

The quantitative age framework and ventilation rates established in this study provide a crucial baseline dataset. This baseline is essential for detecting future changes in ocean circulation and biogeochemical cycles, and will serve to validate the next generation of climate and ocean models.

This study provides a quantitative, basin-scale assessment of Atlantic water mass ages using a multi-tracer approach. However, several methodological assumptions should be considered when interpreting the results. First, the calculated ages rely on the assumption of a steady-state circulation and an Inverse Gaussian Transit Time Distribution (IG-TTD) with a fixed mixing ratio ($\Delta/\Gamma = 1$). Consequently, the mean-age and mode-age presented in this study are linearly related ($\tau_{mode} \approx 0.162 \cdot \Gamma$) and do not provide independent statistical information; they are shown together solely for conceptual comparison of their different physical interpretations (integrative vs. advective timescales). While this is a necessary and common simplification for basin-scale analysis, regional deviations from this idealized transport are likely. Second, the complementary use of tracers (CFC-12, SF_6, ^{39}Ar) mitigates but does not fully eliminate the inherent uncertainties associated with each method, particularly in deep layers with very low tracer concentrations. Finally, the apparent oxygen utilization rates (OUR) derived here represent integrated rates along flow paths and are subject to the same age estimation uncertainties.

Notwithstanding these limitations, the comprehensive age and ventilation maps presented here establish a baseline of the contemporary Atlantic Ocean ventilation structure. This dataset can serve to validate and constrain the next generation of ocean circulation and biogeochemical models. Furthermore, by quantifying current ventilation timescales and their spatial patterns, this work provides a reference frame against which future observational studies can detect changes in ocean circulation and ventilation in response to climatic forcing.

Author contributions. ML designed the research study and conducted the analysis. ML and TT interpreted the results and wrote the paper.

Competing interests. The contact author has declared that none of the authors has any competing interests.

Acknowledgements

This work is based on the comprehensive and detailed data from the GLODAP data product throughout the past few decades. In particular, we are grateful to the efforts from all the scientists and crews on cruises, who generated funding and dedicated time on committing the collection of data. We also would like to thank the working groups of GLODAP for their support and information of the collation, quality control and publishing of data. Their contributions and selfless sharing are prerequisites for the completion of this work. Thank all the colleagues from the School of Environmental Science and Engineering, Xiamen University of Technology for their support in my research work. In addition, we are grateful to Dr. Tim Stöven for his support and advices in running calculating programs of water mass ages. Thanks also goes to Prof. Minggang Cai and his research group at the College of Ocean and Earth Sciences, Xiamen University for the help and support during Mian Liu's postdoctoral work.

Financial support. The authors gratefully thank the Research Projects for Overseas Scholars in Xiamen City (No. 0108/50103250009); Research Start-up Project for the Introduction (Cultivation) of High-level Talents of Xiamen University of Technology (No. YKJ23021R); National Natural Science Foundation of China (No. 22106128) and the Xiamen University of Technology National Natural Science Foundation of China Training Programme for Excellence (No. XPYM2409). Mian Liu received support from the China Scholarship Council (CSC) to support the PhD study at GEOMAR Helmholtz Centre for Ocean Research Kiel, Germany.

References

Armour, K. C., J. Marshall, J. R. Scott, A. Donohoe, and E. R. Newsom: Southern Ocean warming delayed by circumpolar upwelling and equatorward transport, Nature Geoscience, 9(7), 549-554, doi:10.1038/ngeo2731, 2016.

Bender, M. L.: The $\delta^{18}O$ of dissolved O_2 in seawater: A unique tracer of circulation and respiration in the deep sea, Journal of Geophysical Research: Oceans, 95(C12), 22243-22252, doi:https://doi.org/10.1029/JC095iC12p22243, 1990.

Bjerknes, J.: Atlantic Air-Sea Interaction, in Advances in Geophysics, edited by H. E. Landsberg and J. Van Mieghem, pp. 1-82, Elsevier, doi:https://doi.org/10.1016/S0065-2687(08)60005-9, 1964.

Bryden, H. L., H. R. Longworth, and S. A. Cunningham: Slowing of the Atlantic meridional overturning circulation at 25 degrees N, Nature, 438(7068), 655-657, doi:10.1038/nature04385, 2005.

Bullister, J. L., and R. F. Weiss: Anthropogenic Chlorofluoromethanes in the Greenland and Norwegian Seas, Science, 221(4607), 265-268, doi:10.1126/science.221.4607.265, 1983.

Bullister, J. L., D. P. Wisegarver, and F. A. Menzia: The solubility of sulfur hexafluoride in water and seawater, Deep Sea Research Part I: Oceanographic Research Papers, 49(1), 175-187, doi:10.1016/s0967-0637(01)00051-6, 2002.

Clark, P. U., J. D. Shakun, P. A. Baker, P. J. Bartlein, S. Brewer, E. Brook, A. E. Carlson, H. Cheng, D. S. Kaufman, and Z. Liu: Global climate evolution during the last deglaciation, Proceedings of the National Academy of Sciences, 109(19), E1134-E1142, doi:10.1073/pnas.1116619109, 2012.

Dickson, R. R., and J. Brown: The production of North Atlantic Deep Water: Sources, rates, and pathways, Journal of Geophysical Research: Oceans, 99(C6), 12319-12341, doi:10.1029/94jc00530, 1994.

Doney, S. C., and J. L. Bullister: A chlorofluorocarbon section in the eastern North Atlantic, Deep-Sea Res, 39(11-12A), 1857-1883, doi:10.1016/0198-0149(92)90003-c, 1992.

Fine, R. A.: Observations of CFCs and SF_6 as Ocean Tracers, in Annual Review of Marine Science, Vol 3, edited by C. A. Carlson and S. J. Giovannoni, pp. 173-195, doi:10.1146/annurev.marine.010908.163933, 2011.

Gammon, R. H., J. Cline, and D. Wisegarver: Chlorofluoromethanes in the northeast Pacific Ocean: Measured vertical distributions and application as transient tracers of upper ocean mixing, Journal of Geophysical Research-Oceans, 87(NC12), 9441-9454, doi:10.1029/JC087iC12p09441, 1982.

Hall, M. M., and H. L. Bryden: Direct Estmates and Mechanisms of Ocean Heat-Transport, Deep-Sea Res, 29(3), 339-359, doi:10.1016/0198-0149(82)90099-1, 1982.

Hall, T. M., and R. A. Plumb: Age as a diagnostic of stratospheric transport, Journal of Geophysical Research-Atmospheres, 99(D1), 1059-1070, doi:10.1029/93jd03192, 1994.

Huhn, O., M. Rhein, M. Hoppema, and S. van Heuven: Decline of deep and bottom water ventilation and slowing down of anthropogenic carbon storage in the Weddell Sea, 1984-2011, Deep Sea Research Part I: Oceanographic Research Papers, 76, 66-84, doi:10.1016/j.dsr.2013.01.005, 2013.

Ito, T., A. Nenes, M. S. Johnson, N. Meskhidze, and C. Deutsch: Acceleration of oxygen decline in the tropical Pacific over the past decades by aerosol pollutants, Nature Geoscience, 9(6), 443-447, doi:10.1038/ngeo2717, 2016.

Jenkins, W. J.: Oxygen utilization rates in North Atlantic subtropical gyre and primary production in oligotrophic systems, Nature, 300(5889), 246-248, doi:10.1038/300246a0, 1982.

Jenkins, W. J.: ^{3}H and ^{3}He in the Beta Triangle: Observations of Gyre Ventilation and Oxygen Utilization Rates, Journal of Physical Oceanography, 17(6), 763-783, doi:10.1175/1520-0485(1987)017<0763:Aitbto>2.0.Co;2, 1987.

Jia, Z.-H., P. Zhang, L.-B. Li, Q.-W. Chen, J.-L. Liu, Y.-G. Liu, Q. Wu, Y. Yang, L.-T. Sun G.-M. Yang, W. Jiang, Z.-T. Lu: Stability and reliability study of an ^{39}Ar enrichment system for accurate ^{39}Ar dating, Nuclear Instruments and Methods in Physics Research Section A: Accelerators, Spectrometers, Detectors and Associated Equipment, 1075, 170438, doi:https://doi.org/10.1016/j.nima.2025.170438, 2025.

Karstensen, J., and M. Tomczak, Ventilation processes and water mass ages in the thermocline of the southeast Indian Ocean, Geophysical Research Letters, 24(22), 2777-2780, doi:10.1029/97gl02708, 1997.

Karstensen, J., and M. Tomczak: Age determination of mixed water masses using CFC and oxygen data, Journal of Geophysical Research-Oceans, 103(C9), 18599-18609, doi:10.1029/98jc00889, 1998.

Karstensen, J., L. Stramma, and M. Visbeck: Oxygen minimum zones in the eastern tropical Atlantic and Pacific oceans, Progress in Oceanography, 77(4), 331-350, doi: 10.1016/j.pocean.2007.05.009, 2008.

Kirchner, K., M. Rhein, S. Huttl-Kabus, and C. W. Böning: On the spreading of South Atlantic Water into the Northern Hemisphere, Journal of Geophysical Research-Oceans, 114, doi:10.1029/2008jc005165, 2009.

Koeve, W., and P. Kähler: Oxygen utilization rate (OUR) underestimates ocean respiration: A model study, Global Biogeochemical Cycles, 30(8), 1166-1182, doi:10.1002/2015gb005354, 2016.

Kuhlbrodt, T., A. Griesel, M. Montoya, A. Levermann, M. Hofmann, and S. Rahmstorf: On the driving processes of the Atlantic meridional overturning circulation, Reviews of Geophysics, 45(1), doi:10.1029/2004rg000166, 2007.

Lauvset, S. K, R. M. Key, A. Olsen, S. van Heuven, A. Velo, X. Lin, C. Schirnick, A. Kozyr, T. Tanhua, M. Hoppema, S. Jutterström, R. Steinfeldt, E. Jeansson, M. Ishii, F. F. Pérez, T. Suzuki and S. Watelet. A new global interior ocean mapped climatology: the 1°x1° GLODAP version 2, Earth Syst. Sci. Data, 8, 325–340, https://doi:10.5194/essd-8-325-2016, 2016.

Lauvset, S. K., Lange, N., Tanhua, T., Bittig, H. C., Olsen, A., Kozyr, A., Álvarez, M., Azetsu-Scott, K., Brown, P. J., Carter, B. R., Cotrim da Cunha, L., Hoppema, M., Humphreys, M. P., Ishii, M., Jeansson, E., Murata, A., Müller, J. D., Pérez, F. F., Schirnick, C., Steinfeldt, R., Suzuki, T., Ulfsbo, A., Velo, A., Woosley, R. J., and Key, R. M.: The annual update GLODAPv2.2023: the global interior ocean biogeochemical data product, Earth Syst. Sci. Data, 16, 2047–2072, https://doi.org/10.5194/essd-16-2047-2024, 2024.

Li, Q., England, M. H., Hogg, A. M., Rintoul, S. R., & Morrison, A. K., Abyssal ocean overturning slowdown and warming driven by Antarctic meltwater. Nature, 615, (7954), 841-847, 2023.

Liu, M., and T. Tanhua: Water masses in the Atlantic Ocean: characteristics and distributions, Ocean Science, 17(2), 463-486, doi:10.5194/os-17-463-2021, 2021.

Maiss, M., L. P. Steele, R. J. Francey, P. J. Fraser, R. L. Langenfelds, N. B. A. Trivett, and I. Levin: Sulfur hexafluoride - A powerful new atmospheric tracer, Atmospheric Environment, 30(10-11), 1621-1629, doi:10.1016/1352-2310(95)00425-4, 1996.

Morrison, A. K., T. L. Frolicher, and J. L. Sarmiento: Upwelling in the Southern Ocean, Physics Today, 68(1), 27-32, doi:10.1063/pt.3.2654, 2015.

Olsen, A., R. M. Key, S. van Heuven, S. K. Lauvset, A. Velo, X. Lin, C. Schirnick, A. Kozyr, T. Tanhua, M. Hoppema, S. Jutterström, R. Steinfeldt, E. Jeansson, M. Ishii, F. F. Pérez and T. Suzuki. The Global Ocean Data Analysis Project version 2 (GLODAPv2) – an internally consistent data product for the world ocean, Earth Syst. Sci. Data, 8, 297–323, https://doi:10.5194/essd-8-297-2016, 2016.

Orsi, A. H., G. C. Johnson, and J. L. Bullister: Circulation, mixing, and production of Antarctic Bottom Water, Progress in Oceanography, 43(1), 55-109, doi:10.1016/s0079-6611(99)00004-X, 1999.

Patara, L., C. W. Böning, and T. Tanhua: Multidecadal Changes in Southern Ocean Ventilation since the 1960s Driven by Wind and Buoyancy Forcing, Journal of Climate, 34(4), 1485-1502, doi:10.1175/Jcli-D-19-0947.1, 2021.

Purkey, S. G., and G. C. Johnson: Warming of Global Abyssal and Deep Southern Ocean Waters between the 1990s and 2000s: Contributions to Global Heat and Sea Level Rise Budgets, Journal of Climate, 23(23), 6336-6351, doi:10.1175/2010jcli3682.1, 2010.

Pytkowicx, R. M.: On the apparent oxygen utilization and the preformed phosphate in the oceans1, Limnology and Oceanography, 16(1), 39-42, https://doi.org/10.4319/lo.1971.16.1.0039, 1971.

Rahmstorf, S.: The Great Ocean Conveyor: Discovering the Trigger for Abrupt Climate Change, Nature, 464(7289), 681-681, doi:10.1038/464681a, 2010.

Redfield, A. C.: The processes determining the concentration of oxygen, phosphate and other organic derivatives within the depths of the Atlantic Ocean, Pap. Phys. Oceanogr. Meteorol. Mass. Inst. Technol. Woods Hole Oceanogr. Inst., 9, 1–22, https://doi.org/10.1575/1912/1053, 1942.

Redfield, A. C., B. H. Ketchum, F. A. Richards, The influence of organisms on the composition of seawater, The Sea. Ideas and Observations on Progress in the Study of the Seas M. N. Hill, 26–77, John Wiley, New York, 1963.

Sandström, J. W.: Dynamishce versuche mit merrwasser. Annalen der Hydrographie und Maritimen Meteorologie, 36, 6–23, 1908.

Sandström, J. W.: Meteorologische studien im Schwedischen Hochgebirge. Göteborgs Kungl. Vetenskaps- och Vitterhetssamhälles Handlingar, 17, 1–48, 1916.

Schmidtko, S., L. Stramma, and M. Visbeck: Decline in global oceanic oxygen content during the past five decades, Nature, 542(7641), 335-339, doi:10.1038/nature21399, 2017.

Schneider, A., T. Tanhua, A. Kortzinger, and D. W. R. Wallace: High anthropogenic carbon content in the eastern Mediterranean, Journal of Geophysical Research-Oceans, 115, doi:10.1029/2010jc006171, 2010.

Skinner, L. C., F. Primeau, E. Freeman, M. de la Fuente, P. A. Goodwin, J. Gottschalk, E. Huang, I. N. McCave, T. L. Noble, and A. E. Scrivner: Radiocarbon constraints on the glacial ocean circulation and its impact on atmospheric CO_2, Nature Communications, 8, doi:10.1038/ncomms16010, 2017.

Sonnerup, R. E., Quay, P. D., and Bullister, J. L.: Thermocline ventilation and oxygen utilization rates in the subtropical North Pacific based on CFC-11 and CFC-12 measurements from 1991 to 2000, J. Geophys. Res., 106, 9259–9287, https://doi.org/10.1029/1999JC000086, 2001.

Sonnerup, R. E., S. Mecking, and J. L. Bullister: Transit time distributions and oxygen utilization rates in the Northeast Pacific Ocean from chlorofluorocarbons and sulfur hexafluoride, Deep-Sea Res Pt I, 72, 61-71, doi:10.1016/j.dsr.2012.10.013, 2013.

Sonnerup, R. E., S. Mecking, J. L. Bullister, and M. J. Warner: Transit time distributions and oxygen utilization rates from chlorofluorocarbons and sulfur hexafluoride in the Southeast Pacific Ocean, Journal of Geophysical Research-Oceans, 120(5), 3761-3776, doi:10.1002/2015jc010781, 2015.

Stanley, R. H. R., S. C. Doney, W. J. Jenkins, and D. E. Lott: Apparent oxygen utilization rates calculated from tritium and helium-3 profiles at the Bermuda Atlantic Time-series Study site, Biogeosciences, 9(6), 1969-1983, doi:10.5194/bg-9-1969-2012, 2012.

Stöven, T., and T. Tanhua: Ventilation of the Mediterranean Sea constrained by multiple transient tracer measurements, Ocean Science, 10(3), 439-457, doi:10.5194/os-10-439-2014, 2014.

Sverdrup, H. U.: The unity of the sciences of the sea, Sigma Xi Quarterly, 28(3), 105-115, https://www.jstor.org/stable/23049117, 1940.

Talley, L.: Antarctic Intermediate Water in the South Atlantic, in The South Atlantic: Present and Past Circulation, edited by G. Wefer, W. H. Berger, G. Siedler and D. J. Webb, pp. 219-238, Springer Berlin Heidelberg, Berlin, Heidelberg, doi:10.1007/978-3-642-80353-6_11, 1996.

Talley, L.: Closure of the Global Overturning Circulation Through the Indian, Pacific, and Southern Oceans: Schematics and Transports, Oceanography, 26(1), 80-97, doi:10.5670/oceanog.2013.07, 2013.

Talley, L., R. Feely, B. Sloyan, R. Wanninkhof, M. Baringer, J. Bullister, C. Carlson, S. Doney, R. Fine, and E. Firing, N. Gruber, D.A. Hansell, M. Ishii, G.C. Johnson, K. Katsumata, R.M. Key, M. Kramp, C. Langdon, A.M. Macdonald, J.T. Mathis, E.L. McDonagh, S. Mecking, F.J. Millero, C.W. Mordy, T. Nakano, C.L. Sabine, W.M. Smethie, J.H. Swift, T. Tanhua, A.M. Thurnherr, M.J. Warner, and J.-Z. Zhang: Changes in ocean heat, carbon content, and ventilation: A review of the first decade of GO-SHIP global repeat hydrography, Annual review of marine science, 8, 185-215, https://doi.org/10.1146/annurev-marine-052915-100829, 2016.

Tamsitt, V., H. F. Drake, A. K. Morrison, L. D. Talley, C. O. Dufour, A. R. Gray, S. M. Griffies, M. R. Mazloff, J. L. Sarmiento, J. Wang, W. Weijer: Spiraling pathways of global deep waters to the surface of the Southern Ocean, Nature Communications, 8(1), 172, doi:10.1038/s41467-017-00197-0, 2017.

Tanhua, T., A. Biastoch, A. Kortzinger, H. Luger, C. Boning, and D. W. R. Wallace: Changes of anthropogenic CO_2 and CFCs in the North Atlantic between 1981 and 2004, Global Biogeochemical Cycles, 20(4), doi:10.1029/2006gb002695 , 2006.

Tanhua, T., D. W. Waugh, and D. W. R. Wallace: Use of SF_6 to estimate anthropogenic CO2 in the upper ocean, Journal of Geophysical Research-Oceans, 113(C4), doi:10.1029/2007jc004416, 2008.

Tanhua, T., D. W. Waugh, and J. L. Bullister: Estimating changes in ocean ventilation from early 1990s CFC-12 and late 2000s SF_6 measurements, Geophysical Research Letters, 40(5), 927-932, doi:10.1002/grl.50251, 2013.

Tanhua, T., and M. Liu: Upwelling velocity and ventilation in the Mauritanian upwelling system estimated by CFC-12 and SF_6 observations, Journal of Marine Systems, 151, 57-70, doi:10.1016/j.jmarsys.2015.07.002, 2015.

Thiele, G., and J. L. Sarmiento: Tracer Dating and Ocean Ventilation, Journal of Geophysical Research-Oceans, 95(C6), 9377-9391, doi:10.1029/JC095iC06p09377, 1990.

Thomas, J. L., D. W. Waugh, and A. Gnanadesikan: Relationship between Age and Oxygen along Line W in the Northwest Atlantic Ocean, Ocean Science Journal, 55(2), 203-217, doi:10.1007/s12601-020-0019-5, 2020.

Tomczak, M.: Some historical, theoretical and applied aspects of quantitative water mass analysis, Journal of Marine Research, 57(2), 275-303, doi:10.1357/002224099321618227, 1999.

Tseitlin, V.: Depth dependence of oxygen utilization rate, OKEANOLOGIYA, 32(2), 264-269, 1992.

van Heuven, S., M. Hoppema, O. Huhn, H. A. Slagter, and H. J. W. de Baar: Direct observation of increasing CO2 in the Weddell Gyre along the Prime Meridian during 1973-2008, Deep-Sea Research Part Ii-Topical Studies in Oceanography, 58(25-26), 2613-2635, doi:10.1016/j.dsr2.2011.08.007, 2011.

Wang, W. M., M. G. Cai, P. Huang, H. W. Ke, M. Liu, L. H. Liu, H. X. Deng, B. J. Luo, C. H. Wang, X. H. Zheng, W. Q. Li: Transit Time Distributions and Apparent Oxygen Utilization Rates in Northern South China Sea Using Chlorofluorocarbons and Sulfur Hexafluoride Data, Journal of Geophysical Research-Oceans, 126(8), doi:10.1029/2021jc017535, 2021.

Warner, M. J., and R. F. Weiss: Solubility of Chlorofluorocarbon-11 and Chlorofluorocarbon-12 in water and seawater, Deep-Sea Res, 32(12), 1485-1497, doi:10.1016/0198-0149(85)90099-8, 1985.

Waugh, D. W., T. M. Hall, and T. W. N. Haine: Relationships among tracer ages, Journal of Geophysical Research: Oceans, 108(C5), doi:10.1029/2002jc001325, 2003.

Waugh, D. W., T. W. N. Haine, and T. M. Hall: Transport times and anthropogenic carbon in the subpolar North Atlantic Ocean, Deep Sea Research Part I: Oceanographic Research Papers, 51(11), 1475-1491, doi:10.1016/s0967-0637(04)00145-1, 2004.

Ziska, F., B. Quack, K. Abrahamsson, S. D. Archer, E. Atlas, T. Bell, J. H. Butler, L. J. Carpenter, C. E. Jones, N. R. P. Harris, H. Hepach, K. G. Heumann, C. Hughes, J. Kuss, K. Krüger, P. Liss, R. M. Moore, A. Orlikowska, S. Raimund, C. E. Reeves, W. Reifenhäuser, A. D. Robinson, C. Schall, T. Tanhua, S. Tegtmeier, S. Turner, L. Wang, D. Wallace, J. Williams, H. Yamamoto, S. Yvon-Lewis, and Y. Yokouchi: Global sea-to-air flux climatology for bromoform, dibromomethane and methyl iodide, Atmospheric Chemistry and Physics, 13(17), 8915-8934, doi:10.5194/acp-13-8915-2013, 2013.